ADVANCED SCIENCE
Open Access

# Supporting Information

for *Adv. Sci.*, DOI 10.1002/advs.202305096

A Cell-Penetrant Peptide Disrupting the Transcription Factor CP2c Complexes Induces Cancer-Specific Synthetic Lethality

*Seung Han Son, Min Young Kim, Sungwoo Choi, Ji Sook Kim, Yong Sang Lee, Sangwon Lee, Yeon Ju Lee, Jin Youn Lee, Seol Eui Lee, Young Su Lim, Dae Hyun Ha, Eonju Oh, Young-Bin Won, Chang-Jun Ji, Mi Ae Park, Boram Kim, Kyu Tae Byun, Min Sung Chung, Jaemin Jeong, Dongho Choi, Eun Jung Baek, Eung-Ho Cho, Sang-Bum Kim, A. Reum Je, Hee-Seok Kweon, Hyun Sook Park, Dongsun Park, June Sung Bae, Se Jin Jang, Chae-Ok Yun, Ji Hyung Chae, Jin-Won Lee, Su-Jae Lee, Chan Gil Kim, Ho Chul Kang*, Vladimir N. Uversky* and Chul Geun Kim**

# Supporting Information

## A cell-penetrant peptide disrupting the transcription factor CP2c complexes induces cancer-specific synthetic lethality

Seung Han Son[1]†, Min Young Kim[1]†, Sungwoo Choi[1]†, Ji Sook Kim[1,2], Yong Sang Lee[1], Sangwon Lee[1], Yeon Ju Lee[1], Jin Youn Lee[1], Seol Eui Lee[1], Young Su Lim[1], Dae Hyun Ha[1], Eonju Oh[3], Young-Bin Won[1], Chang-Jun Ji[1], Mi Ae Park[1], Boram Kim[4], Kyu Tae Byun[4], Min Sung Chung[5], Jaemin Jeong[5], Dongho Choi[5], Eun Jung Baek[6], Eung-Ho Cho[7], Sang-Bum Kim[7], A Reum Je[8], Hee-Seok Kweon[8], Hyun Sook Park[9], Dongsun Park[10], June Sung Bae[11], Se Jin Jang[11,12,13], Chae-Ok Yun[3], Ji Hyung Chae[1], Jin-Won Lee[1], Su-Jae Lee[1]‡, Chan Gil Kim[4], Ho Chul Kang[1]‡*, Vladimir N. Uversky[14]*, Chul Geun Kim[1,15]*

Correspondence to: hckang@ajou.ac.kr (H.C.K.), vuversky@usf.edu (V.N.U.), and cgkim@hanyang.ac.kr (C.G.K.)

**This PDF file includes:**

Figure S1 to S27
Table S1 to S4

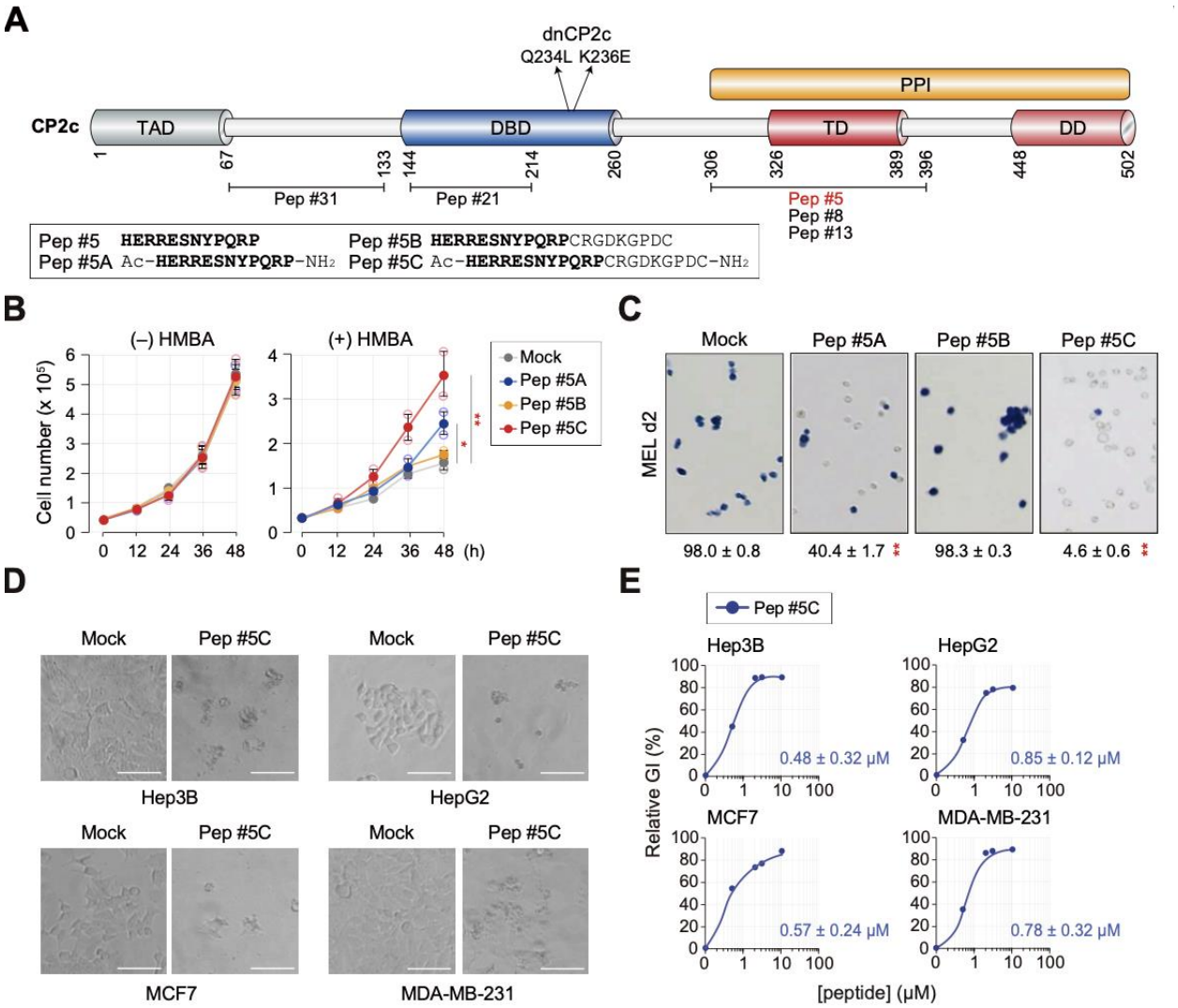


**Figure S1. Targeting CP2c with Pep #5 inhibits HMBA-induced MEL cell differentiation and induces cancer cell death**

A) Schematic diagram showing the functional domains of the CP2c protein where various peptides bind. Amino acid sequences and N- and C-terminal modifications of Pep #5 and its derivatives are displayed in the lower left box. TAD, transactivation domain; DBD, DNA binding domain; TD, tetramerization domain; DD, dimerization domain; PPI, protein-protein interaction; dnCP2c, dominant negative form of human CP2c (Q234L and K236E). B,C) Pep #5 targets CP2c to inhibit HMBA-induced MEL (iMEL) cell differentiation. B) Cell proliferation assays in uninduced MEL (uMEL) and iMEL cells demonstrates effective inhibition of erythroid differentiation by Pep #5C (10 μM). Data are presented as means ± SD of two independent biological replicates. Two-tailed unpaired Student's *t*-tests; $*P < 0.05$, $**P < 0.01$. C) Functional hemoglobin synthesis analysis using benzidine staining. Functional hemoglobin synthesis analysis was performed using benzidine staining, and the percentages of benzidine-positive stained cells were quantified relative to the total cell count. Representative staining images are provided, and below them, the benzidine-positive percentages are reported as means ± SD from two independent biological replicates. Two-tailed unpaired Student's t-tests, $**P < 0.01$. D,E) Pep #5C induces robust growth inhibition and cell death of cancer cells. Cell photographs captured at 96 h after Pep #5C (10 μM) treatment (D) and growth inhibition profiles with $GI_{50}$ values (E) in the representative cancer cells at 96 h after Pep #5C treatment. $GI_{50}$ values estimated from two independent biological replicates.

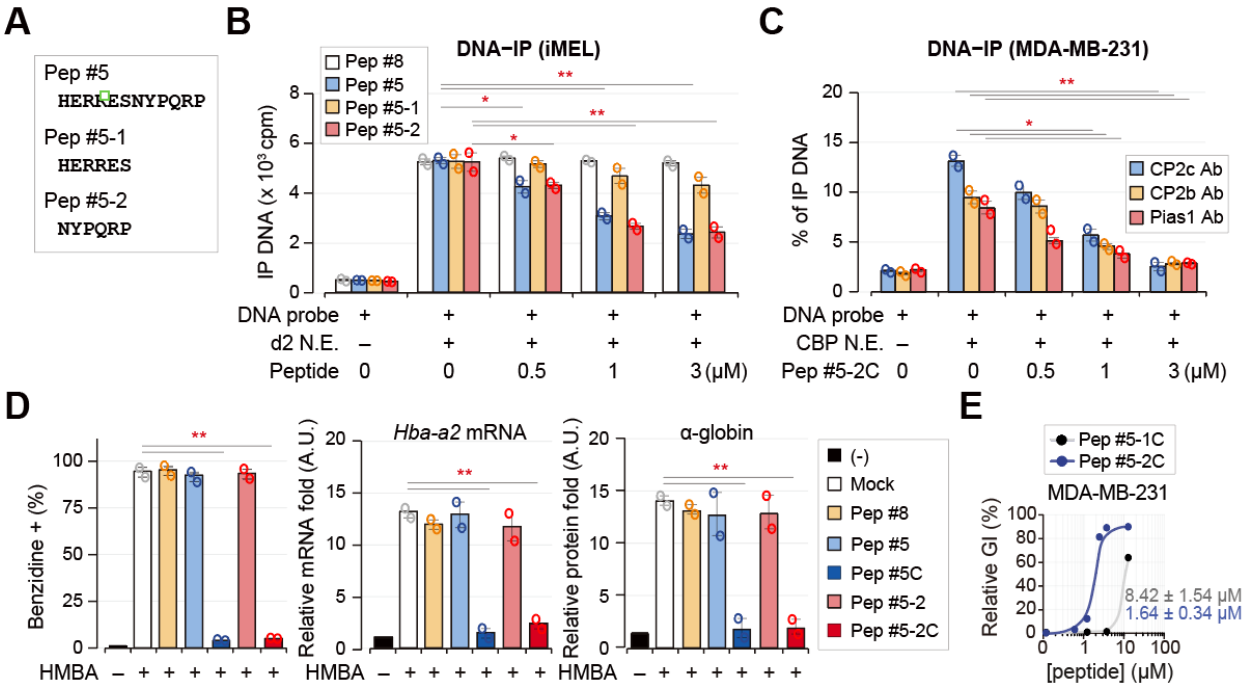


**Figure S2. Pep #5-2, a 6-amino acid peptide corresponding to the C-terminal half of Pep #5, exhibits the same activity as Pep #5**

A-C) Pep #5-2 inhibits the DNA binding activity of CP2c as does by Pep #5. (A) Amino acid sequences of Pep #5 and its derivatives, Pep #5-1 and Pep #5-2. The isotope labeling (B) or biotin labeling (C) was performed on the wildtype *Hba-a2* promoter which were served as a probe in reactions containing nuclear extracts from iMEL cells (day 2) or MDA-MB-231 cells, respectively. Data are presented as means ± SD of two independent biological replicates. Two-tailed unpaired Student's *t*-tests; $^{**}P < 0.01$; $^{*}P < 0.05$. D) Pep #5-2C (Pep #5-2 linked to a cell penetrating peptide, iRGD) efficiently inhibits functional hemoglobin synthesis (left), and *Hba-a2* globin gene expression at both mRNA (middle) and protein (right) levels in iMEL cells. Fractions of benzidine-positive stained cells were counted in MEL cells (n > 100 cells/group) treated with HMBA for 2 days. *Hba-a2* gene expression at mRNA and protein levels were estimated by RT-qPCR and WB, respectively. Data are presented as means ± SD of two independent biological replicates. Two-tailed unpaired Student's *t*-tests; $^{**}P < 0.01$. E) Growth inhibition profiles of MDA-MB-231 cells at 96 h after treatment of Pep #5-1C or Pep #5-2C. $GI_{50}$ values estimated from two independent biological replicates.

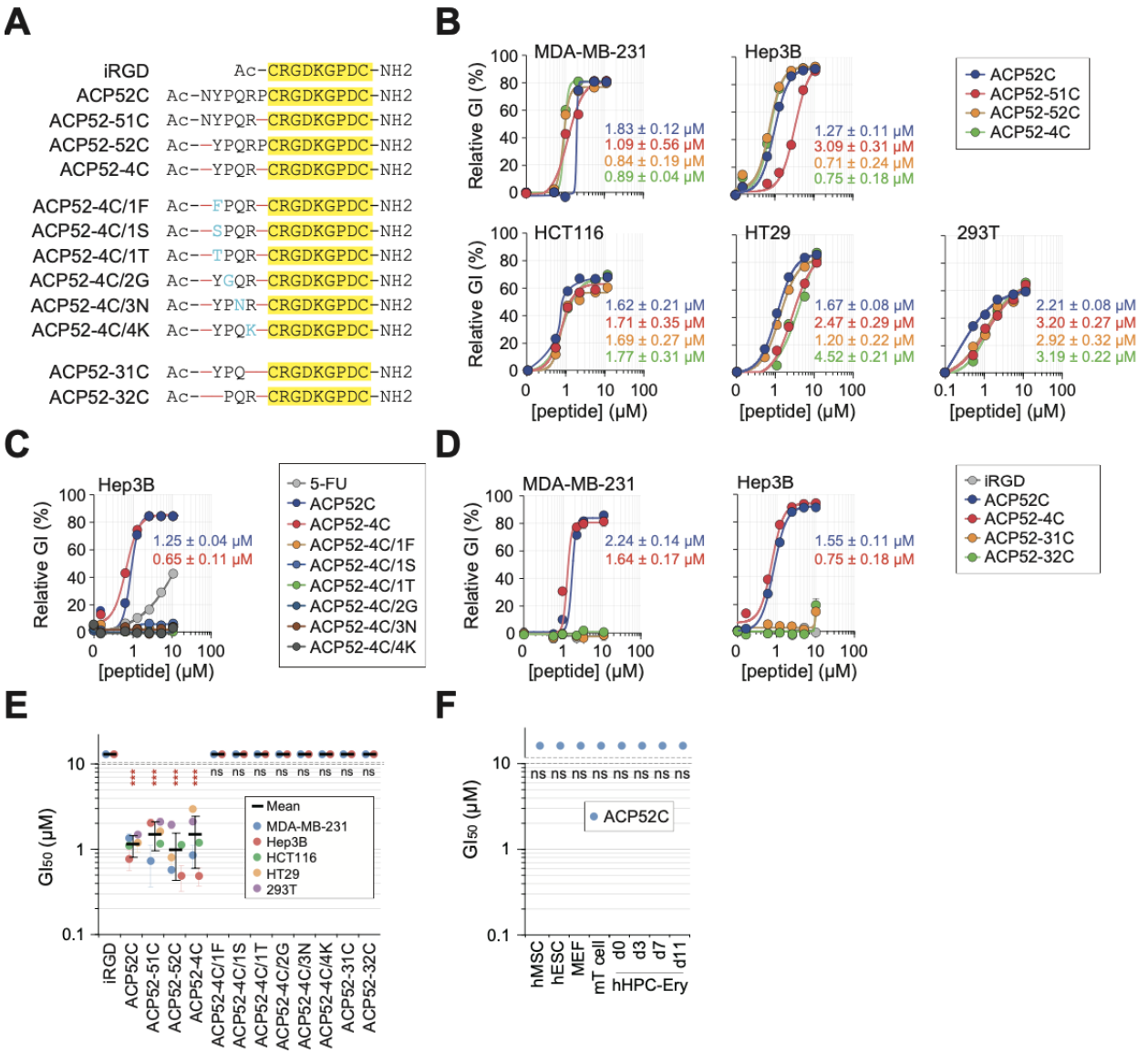


**Figure S3. Anticancer effect of Pep #5-2 truncated and substitution mutants**

A) Names and peptide sequences of each mutant. Peptides corresponding to each Pep #5-2 truncated or substitution mutant are linked to a cell penetration peptide, iRGD (highlighted with yellow boxes). B-E) Cell growth inhibition profiles and $GI_{50}$ values of each mutant in representative cancer cell lines. $GI_{50}$ values estimated from duplicated data are expressed as means ± SD. Data are presented as means ± SD of two independent biological replicates. Anticancer effect of ACP52C, ACP52-51C, ACP52-52C, and ACP52-4C (B), amino acid substitution mutants of ACP52-4C (C), and ACP52C, ACP52-4C, ACP52-31C, and ACP52-32C (D). Cell growth inhibition was tested in cells using MTT assay over peptide dose at 48 h after peptide treatment, and $GI_{50}$ values estimated from duplicated data are expressed as means ± SD. (E) Summary of $GI_{50}$ values of each mutant in representative cancer cell lines. $GI_{50}$ values estimated from duplicated data are expressed as means ± SD. Two-tailed unpaired Student's *t*-tests, ***$P < 0.001$; ns: non-significant. F) $GI_{50}$ values of ACP52C in various normal human and mouse cells, indicating their resistance to ACP52C. hMSC; human mesenchymal stem cells, hESC; human embryonic stem cells, MEF; mouse embryonic fibroblasts, mT cell; mouse T cells, hHPC-Ery; differentiating erythroid cells in vitro from the human $CD34^+$ hematopoietic progenitor cells. Two-tailed unpaired Student's *t*-tests, ns: non-significant.

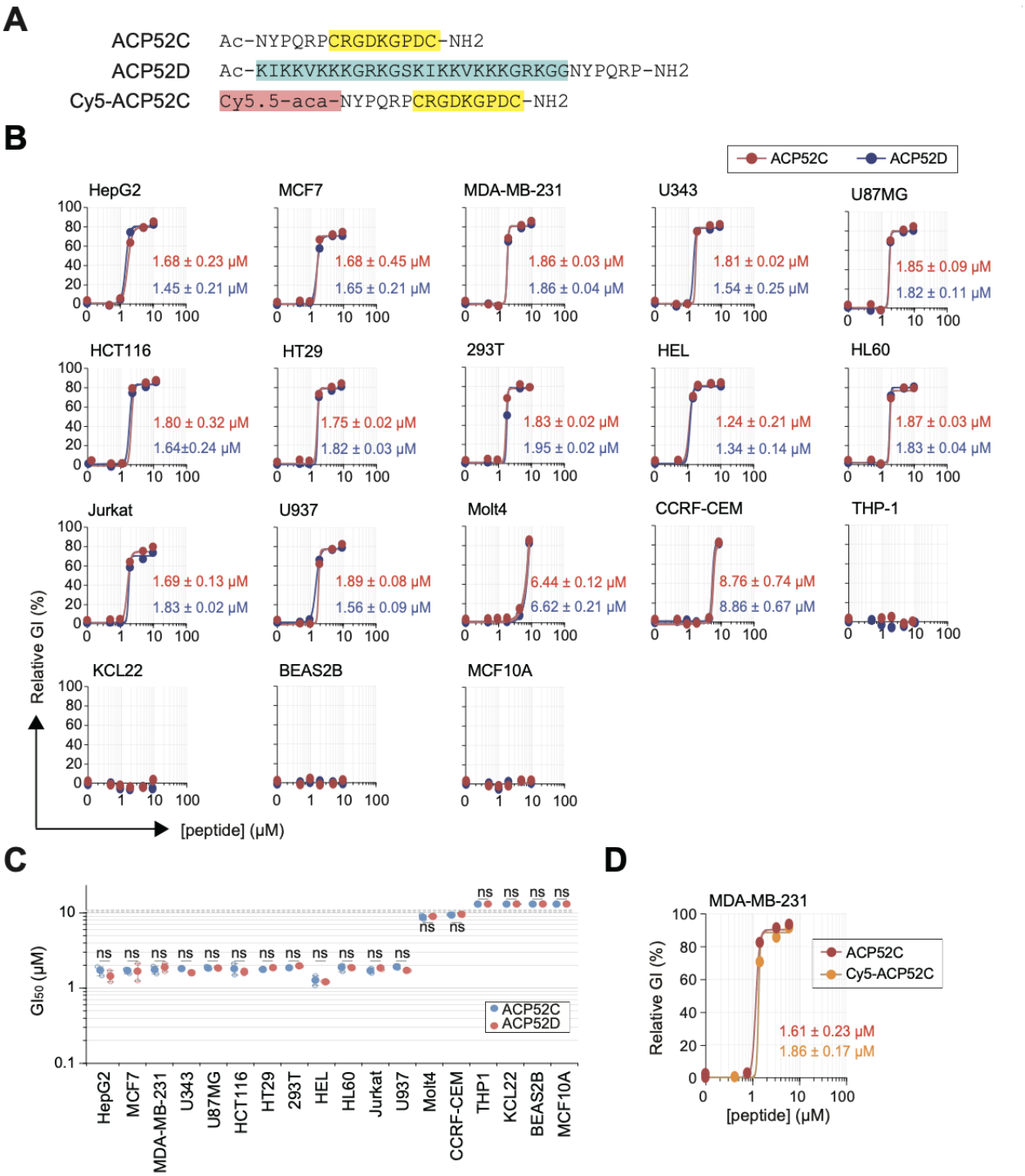


**Figure S4. The ACP52 sequence by itself exhibits anticancer activity irrespective of the attached CPPs**

A) Peptide sequences of ACP52C, ACP52D, and Cy5-ACP52C, with highlighted boxes of yellow, cyan, and salmon for the iRGD or dNP2 CPP, and Cy5 fluorochrome attached by a linker, respectively. B,C) Cell growth inhibition plots and $GI_{50}$ values of ACP52C and ACP52D in various cancer cell lines over peptide dose (B). The summarized $GI_{50}$ values are presented in (C). $GI_{50}$ values estimated from duplicated data are expressed as means ± SD. Two-tailed unpaired Student's *t*-tests, ns: non-significant. Cell growth was assessed from duplicated data at 96 h after peptide treatment using MTT assay and expressed as means ±

SD. Two-tailed unpaired Student's *t*-tests, ns: non-significant. D) Comparative cell growth inhibition curves and $GI_{50}$ values of ACP52C and Cy5-ACP52C. $GI_{50}$ values estimated from duplicated data are expressed as means ± SD.

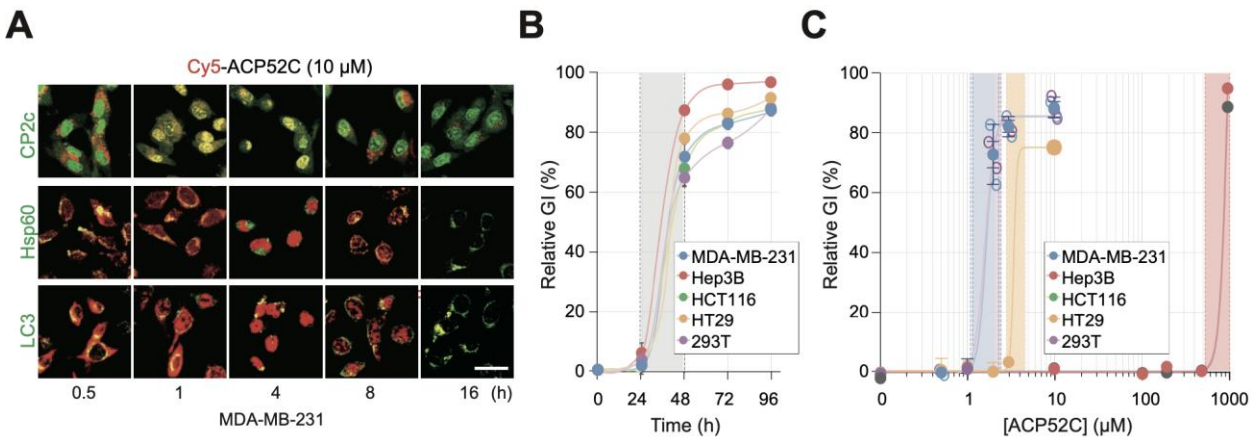


**Figure S5. Prognostic characteristics of ACP52C at the cell level**

A) Time-dependent subcellular localization of ACP52C. Merged confocal microscopy images demonstrating the colocalization of ACP52C with CP2c, the mitochondrial marker Hsp60, or the lysosomal marker LC3 over time following treatment with Cy5-ACP52C. Cy5-ACP52C (10 μM) was supplemented to the culture medium for 30 min in MDA-MB-231 cells, and IF was performed at different time points after replenishing of fresh medium to observe the subcellular localization of ACP52C. Scale bar represents 10 μm. B,C) ACP52C exerts growth inhibition effects on cells at least 48 h after treatment (B) and within a narrow concentration range (C). Growth inhibition profiles of representative cells from duplicated data are depicted at 24, 48, 72, and 96 h (B) or at 96 h (C) after ACP52C treatment.

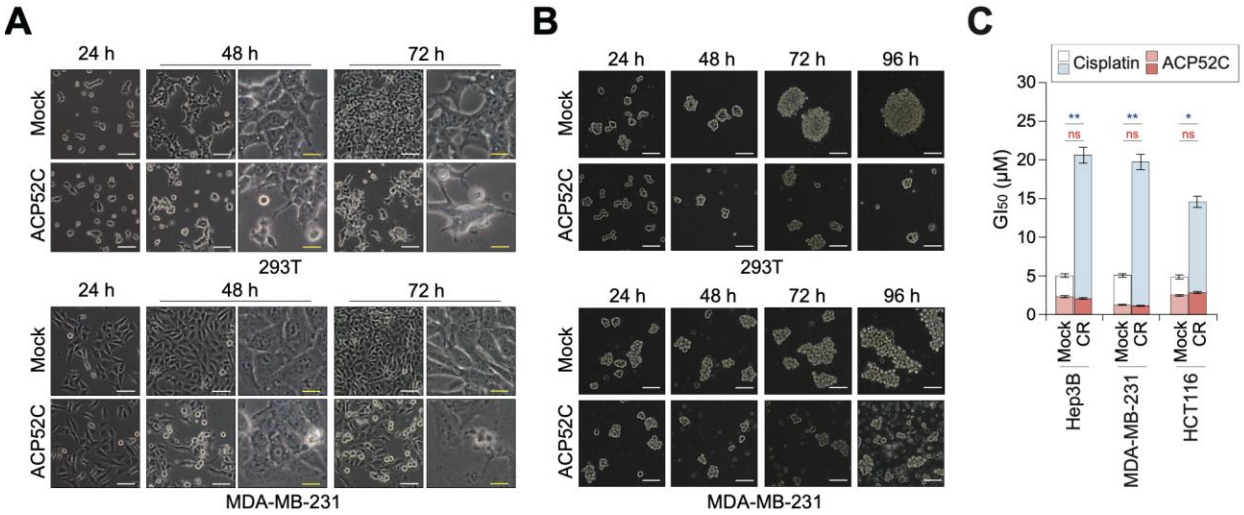


**Figure S6. ACP52C drives cancer cell-specific synthetic lethality**

A,B) ACP52C exerts its anticancer activity on cancer cells independently of the culture condition, whether it's in monolayer (A) or in mammosphere-forming conditions (B). Photographs depict 293T and MDA-MB-231 cells cultured in either monolayer or mammosphere-forming condition over time after treatment of ACP52C (2 μM). Yellow and white scale bars represent 2.5 and 25 μm, respectively. C) ACP52C also exhibits anticancer activity in cisplatin-resistant (CR) cancer cells. $GI_{50}$ values were estimated in various cisplatin-resistant cells and their parent cells. Duplicated data are expressed as means ± SD. Two-tailed unpaired Student's *t*-tests; *, $P < 0.05$; **, $P < 0.01$; ns, non-significant.

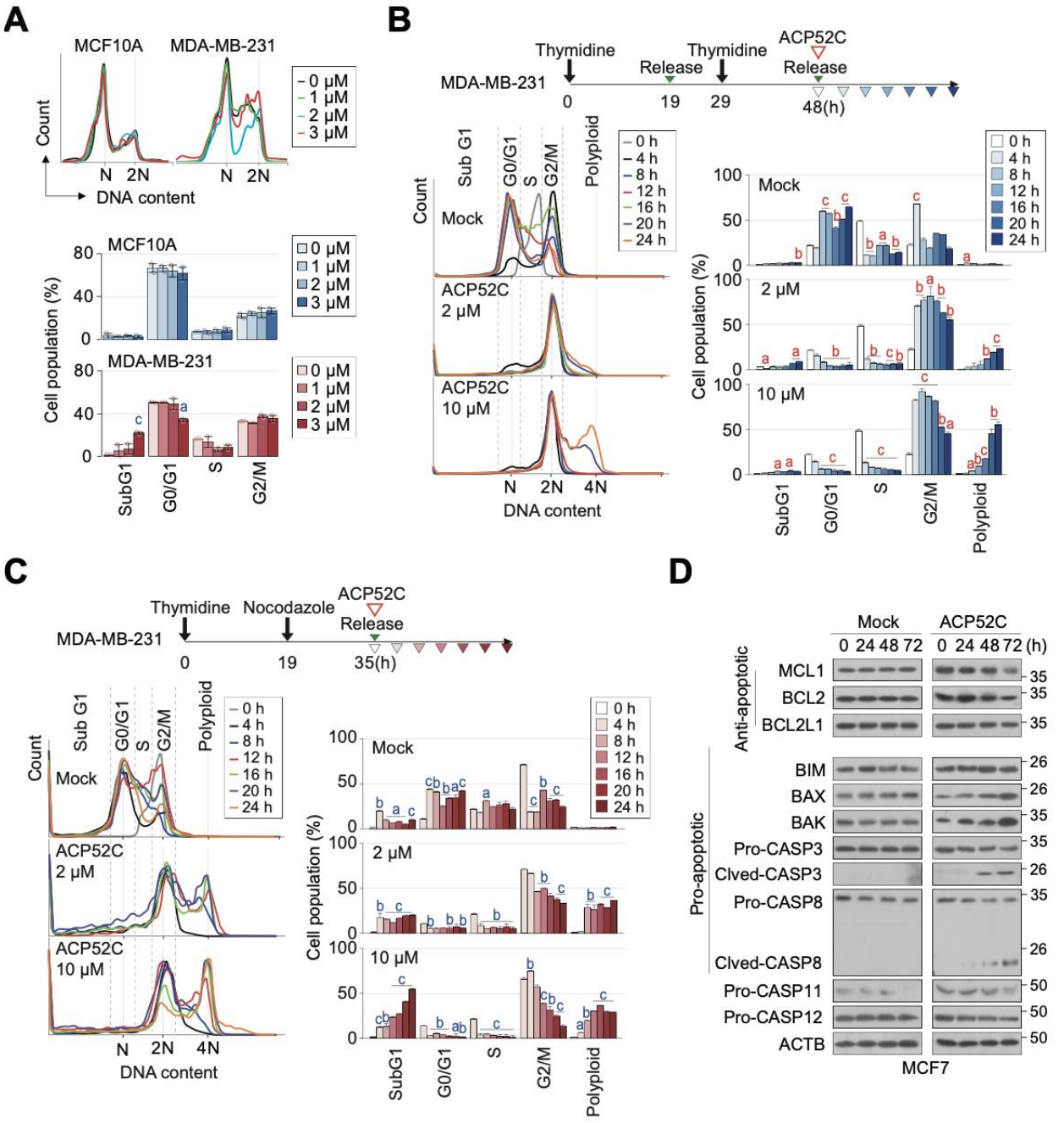


**Figure S7. ACP52C induces G2/M arrest and apoptosis**

A) Effects of ACP52C on the cell cycle in asynchronous populations. Overlay histograms of the cell cycle analyses (upper panel) and the distribution of cells across the cell cycle (lower panel) 24 h after ACP52C treatment over concentration. Duplicated data are expressed as means ± SD. ANOVA test; a, $P < 0.05$; c, $P < 0.001$. B,C) Cell cycle distribution in the synchronized cell populations following ACP52C treatment over time. Experimental schematics (upper panels), overlay histograms of the cell cycle analyses (lower left panels), and cell cycle distribution (lower right panels) illustrate the effects of ACP52C on cell cycle progression in synchronized cells at the G1/S boundary using thymidine double block (B) or at G2/M boundary following nocodazole treatment (C). Duplicated data are expressed as means ± SD. ANOVA test; a, $P < 0.05$; b, $P < 0.01$; c, $P < 0.001$. D) WBs display changes in the expression of apoptotic marker proteins in mock or ACP52C (2 μM)-treated MCF7 cells.

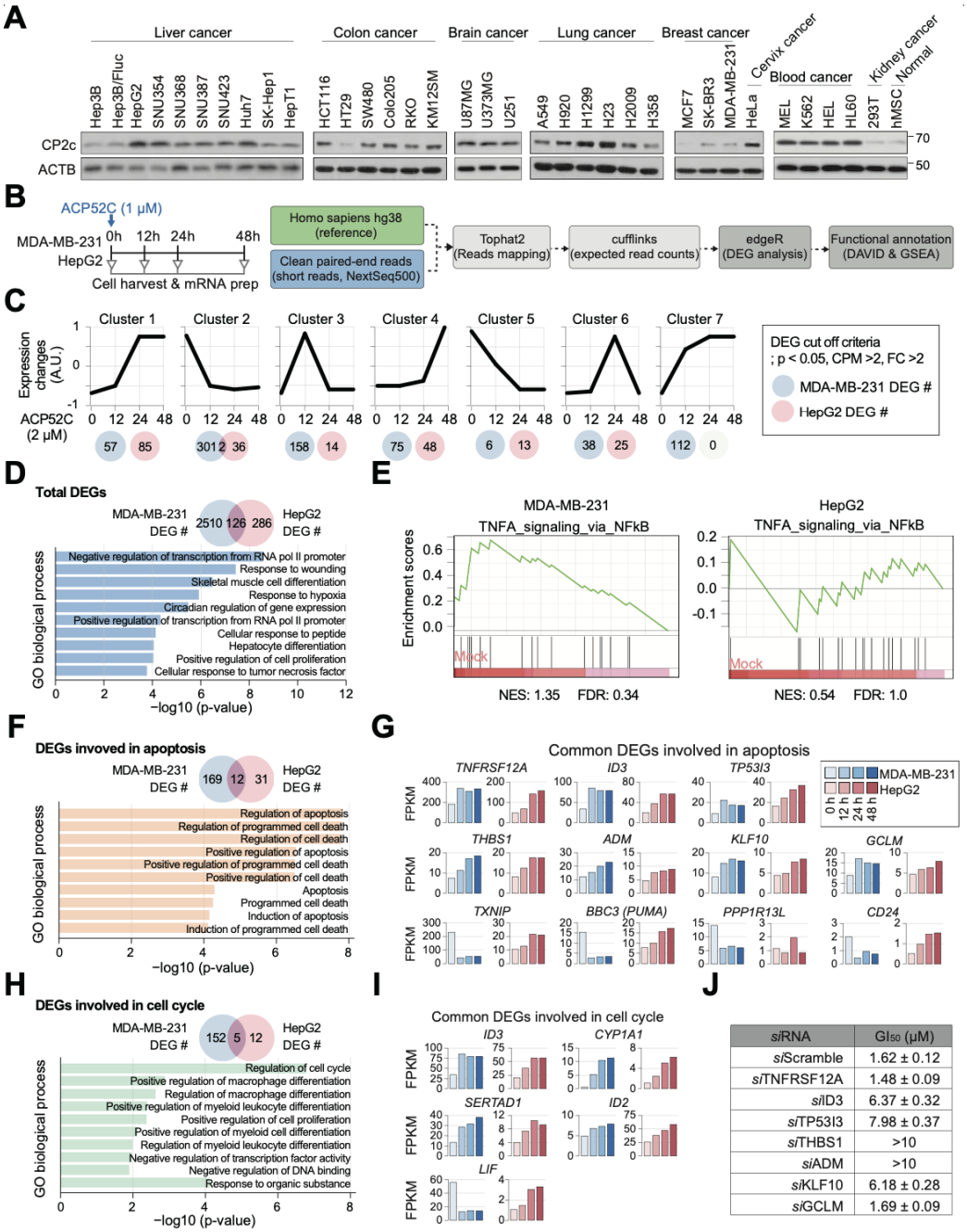


**Figure S8. CP2c transcriptional activity is not involved in ACP52C-mediated G2/M arrest and apoptosis induction**

A) WBs showing elevated CP2c expression in most of cancer cell lines derived from different origins of tumor. B,C) DEG analyses conducted on MDA-MB-231 and HepG2 cells over time after ACP52C treatment. Experimental scheme (B) and identification of DEGs that exhibit similar expression patterns over time in both cell lines (C). D,E) The GO (D) and GSEA (E) analyses conduced on the common DEGs identified in both cell lines following ACP52C treatment. F-J) GO analyses related to apoptosis- (F) and the cell cycle (H) performed on the common DEGs. Histograms depict changes in mRNA expression for DEGs associated with apoptosis (G) and cell cycle (I). $GI_{50}$ values in MDA-MB-231 cells were estimated from two independent biological replicates, 96 h after each DEG-specific siRNA treatment (J).

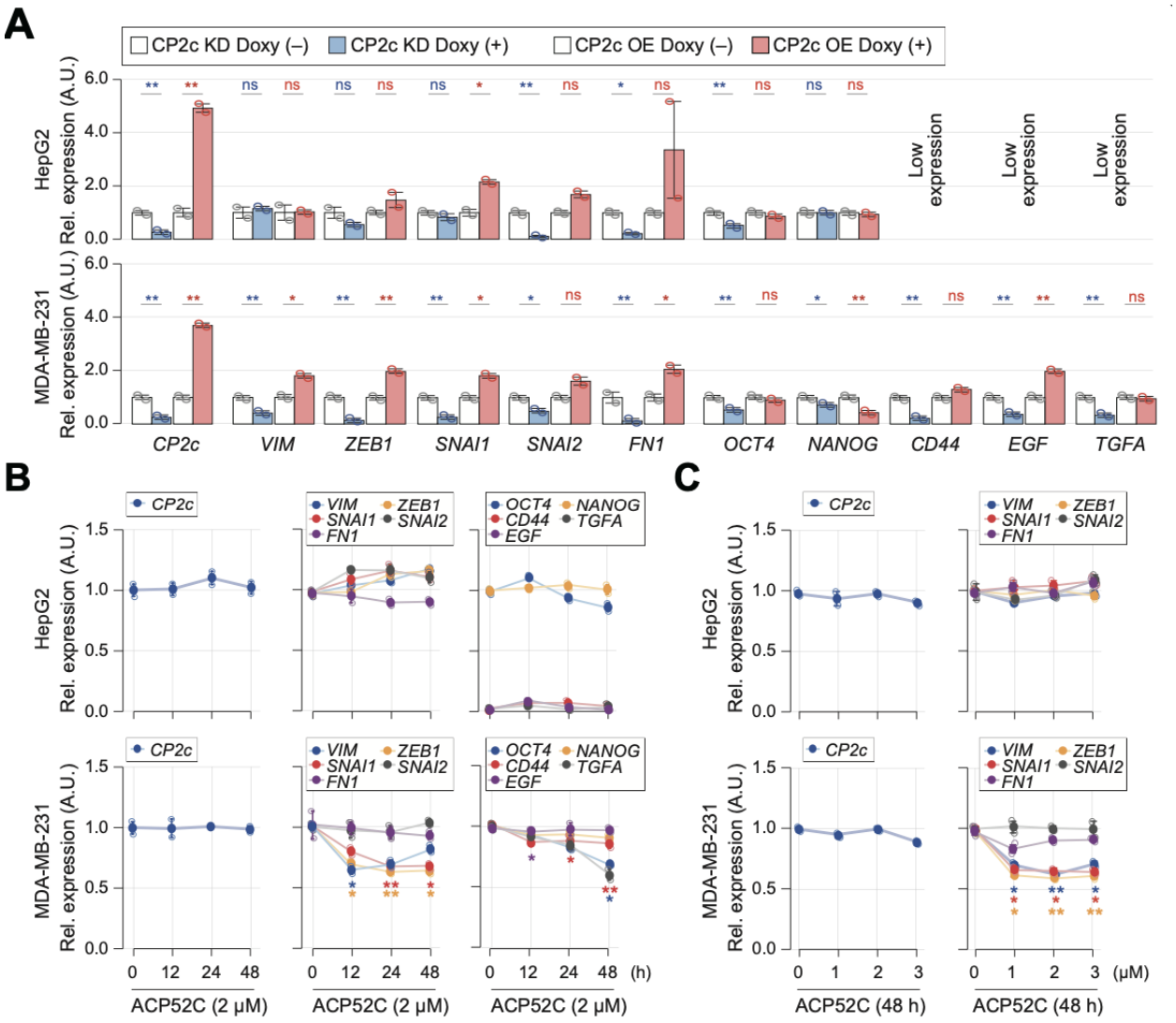


**Figure S9. ACP52C does not affect the expression of EMT-related makers, even though they are transcriptional targets of CP2c**

A-C) RT-qPCR data showing expression changes of EMT-related genes by CP2c OE or KD (A), or ACP52C treatment over time and dose (B,C). Duplicated data are expressed as means ± SD. Two-tailed unpaired Student's *t*-tests; *, P < 0.05; **, *P* < 0.01; ns, non-significant.

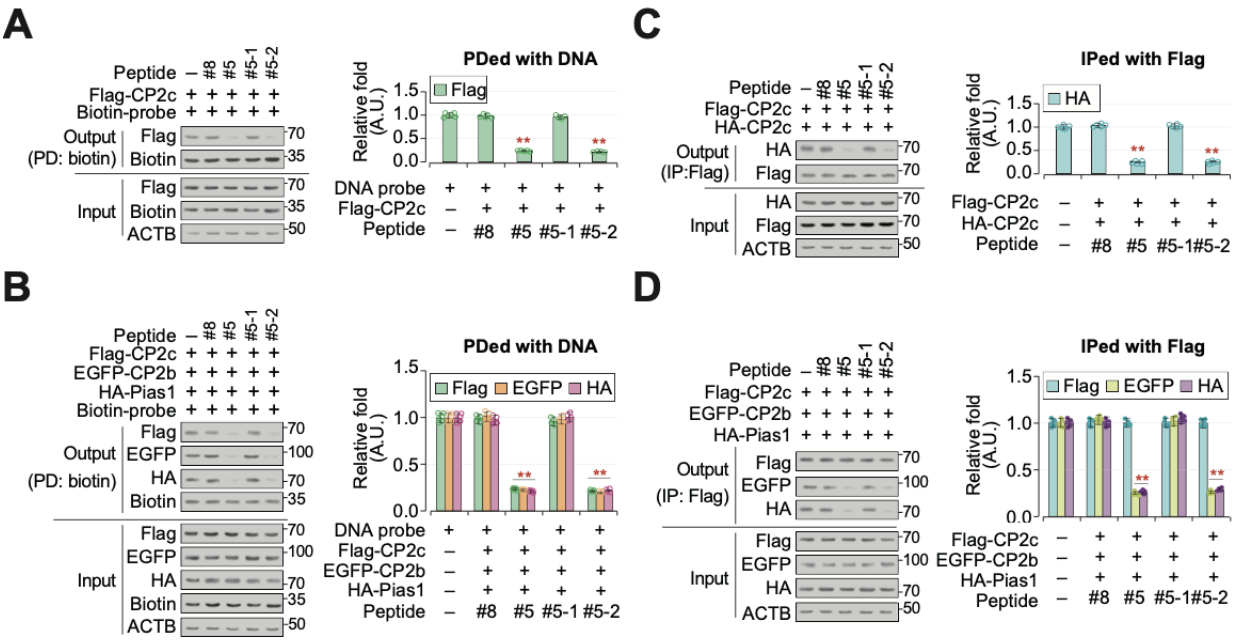


**Figure S10. Pep #5-2 inhibits the DNA binding of CP2c complexes by disrupting CP2c transcription factor complexes**

A-D) Pep #5-2 efficiently inhibits both the DNA binding ability of CP2c complexes and the CP2c complex formation by itself. DNA-pull down (A,B) and co-IP (C,D) assays to the [C4] complex (A,C) and the CBP complexes (B,D). Data are means ± SD of two independent biological replicates. Two-tailed unpaired Student's *t*-tests; $^{**}P < 0.01$.

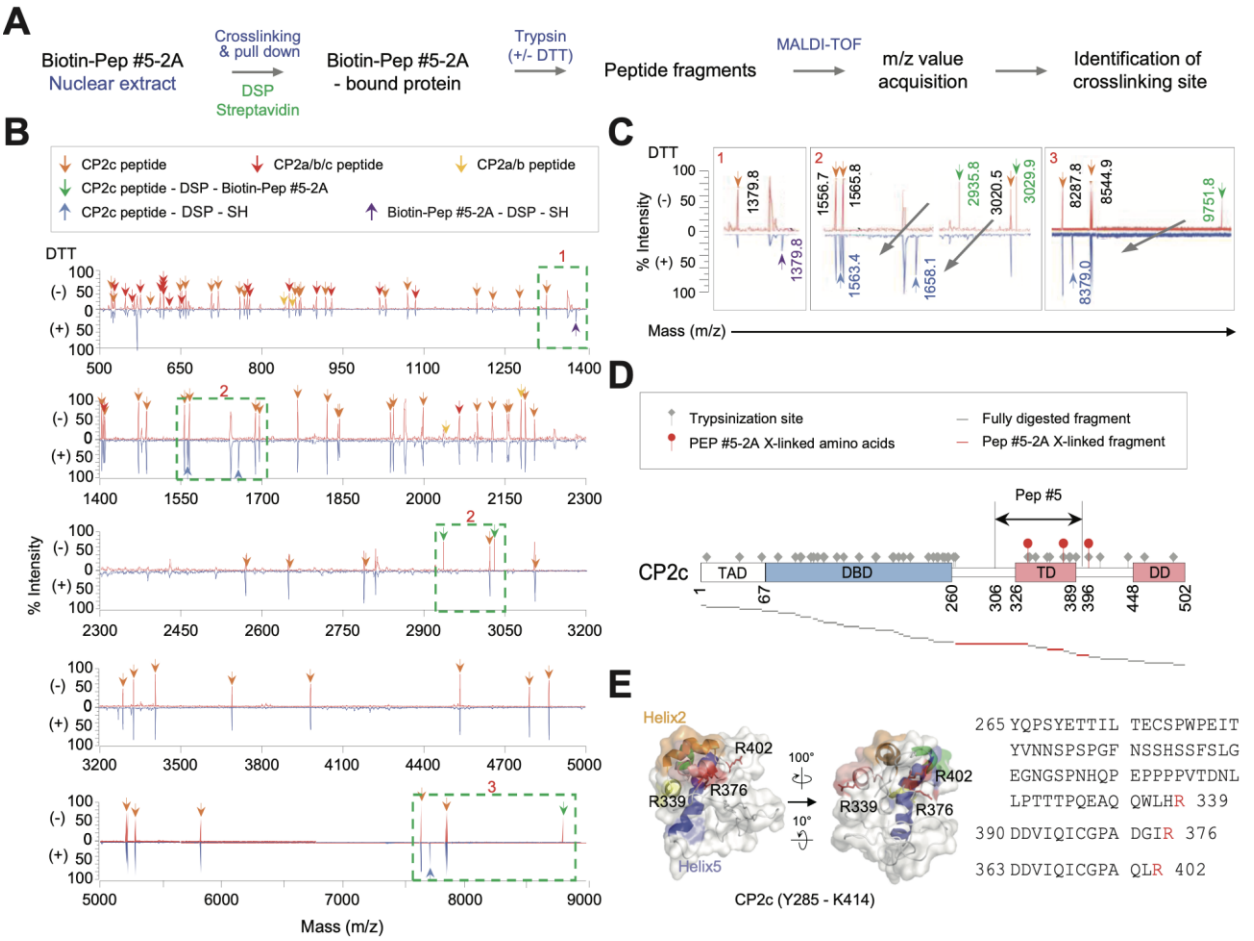


**Figure S11. Identification of Pep #5-2 binding nuclear proteins and their specific crosslinked residues.**

A) Experimental scheme of DSP crosslinking and mass spectrometry analyses to identify nuclear proteins bound to Pep #5-2 and their specific crosslinked residues. B) MALDI-TOF raw peak data showing nuclear protein profiles analyzed in the presence (+) or absence (−) of DTT after DSP crosslinking and pull down with streptavidin beads. Results from two independent experiments were overlaid. C) Highlights of peptide fragment peaks within dotted green rectangles with numbers in (B), indicating the biotin-Pep #5-2A crosslinked CP2c fragments (long arrows) with reduced masses (m/z) upon DTT treatment. Green colored mass (m/z) scores; peptide fragments that disappeared by DTT treatment, blue colored ones; those appeared by DTT treatment. D,E) Pep #5-2 specifically interacts with amino acids on one surface of the CP2c TD. (D) Schematic diagram illustrating biotin-Pep #5-2A crosslinked sites (red filled circles) in the CP2c protein and biotin-Pep #5-2A crosslinked CP2c fragments after trypsin digestion (red horizontal lines). (E) Three-dimensional structure of the CP2c TD domain, with the biotin-Pep #5-2A crosslinked amino acids (R339, R376, and R402) highlighted. Amino acid sequences of each crosslinked peptide fragment containing cross-linked amino acids (red colored letter) are shown on the right side. The TD domain's helixes 1 through 5 are denoted with ribbons in red, orange, yellow, green, and blue, respectively.

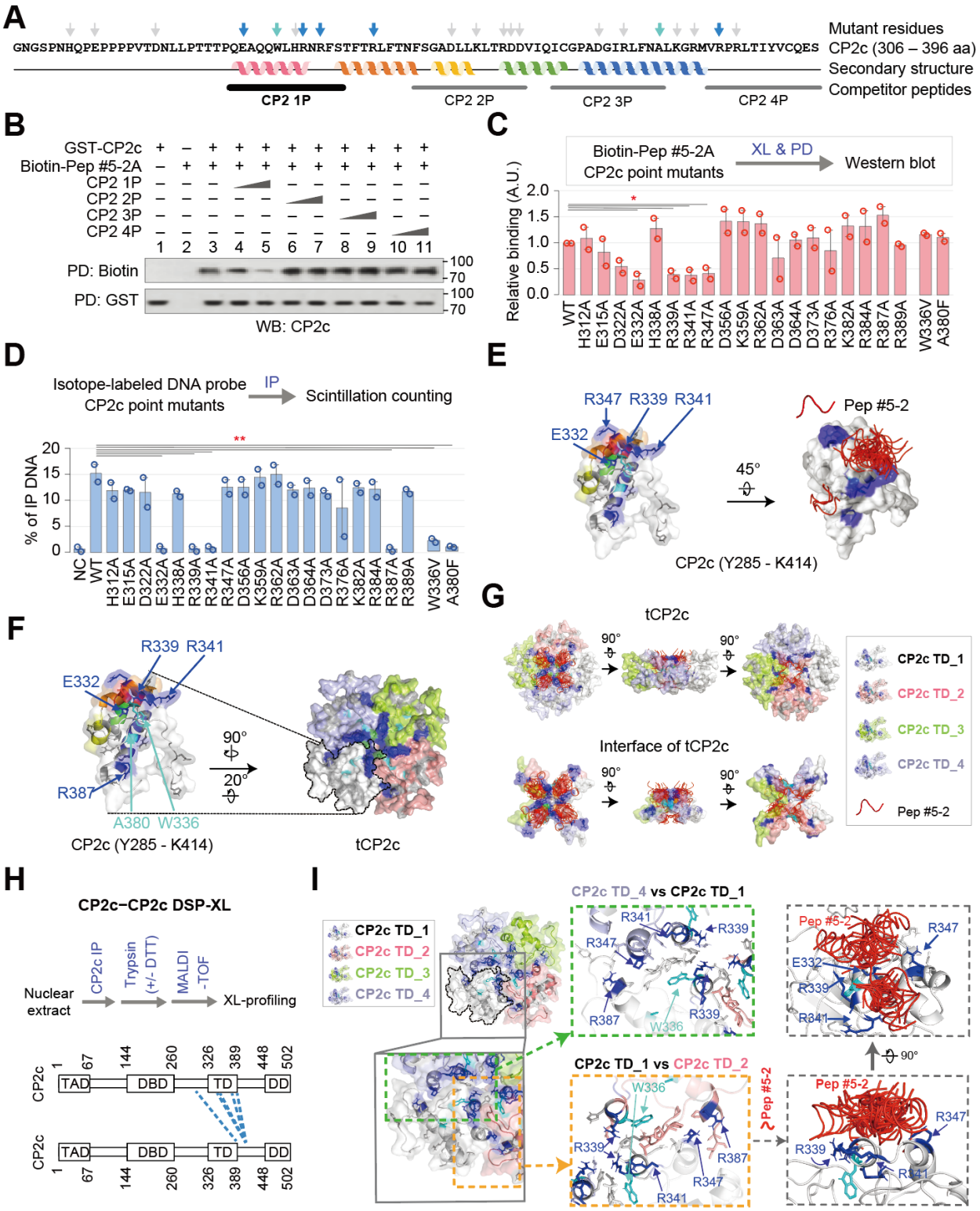


**Figure S12. Pep #5-2 binds to interaction junctions within the tCP2c complex disrupting the formation of the complex**

A) The CP2c TD domain (306 to 396 amino acids) with secondary structural characters, competitor peptides used in (B), and point mutation residues (vertical arrows) used in (C) and (D). Blue- and cyan-colored

vertical arrows indicate the charged residues or additional Ala mutations in non-charged residues important for Pep #5-2 binding and/or for CP2c complex formation, respectively. B) Competition DNA-pull down analyses identifying CP2 1P as a specific inhibitor for DNA binding of CP2c complexes. C,D) Effects of Ala mutant on Pep #5-2 binding (C) and DNA binding (D). Data are represented as means ± SD of two independent biological replicates. Two-tailed unpaired Student's *t*-tests; $*P < 0.05$; $**P < 0.01$. E-G) Structural model of Pep #5-2 binding to the interaction junctions of CP2c TD tetramer. Mapping of the Pep #5-2 binding region and residues important for tCP2c complex formation to the CP2c TD model obtained by I-TASSER and MODELLER (E). A HADDOCK model of the TD tetramer in the tCP2c complex (F), where Pep #5-2 binding occurs in the interaction junctions of CP2c in the complex. Three-dimensional views of the integral CP2c TD tetramer (top) and the interaction junctions among subunits (bottom) in the tCP2c complex, highlighting the Pep #5-2 binding locations (G). H) CP2c interacts each other through residues around TD, as revealed by DSP crosslinking in solution. I) Close-up view of the Pep #5-2-targeting CP2c-CP2c interaction junctions in the [C4] complex. Residues important for [C4] complex formation are in the interface of CP2c TD tetramer, where residues important for Pep #5-2 binding are partially overlapped. Each of CP2c monomers is color-coded in CP2c TD tetramer (top, left). Residues important for Pep #5-2 binding and/or [C4] complex formation are marked by blue (for charged residues) and cyan (for W336 and A380). Orange- and green-colored dotted rectangles are junctions between adjacent CP2c monomer, showing the close-up views of the binding interface between CP2c TD_1 (white) and TD_2 (salmon) and between CP2c TD_1 (white) and TD_4 (light blue) with important residue information. Close-up views of Pep #5-2 binding to CP2c TD_1 is shown (right).

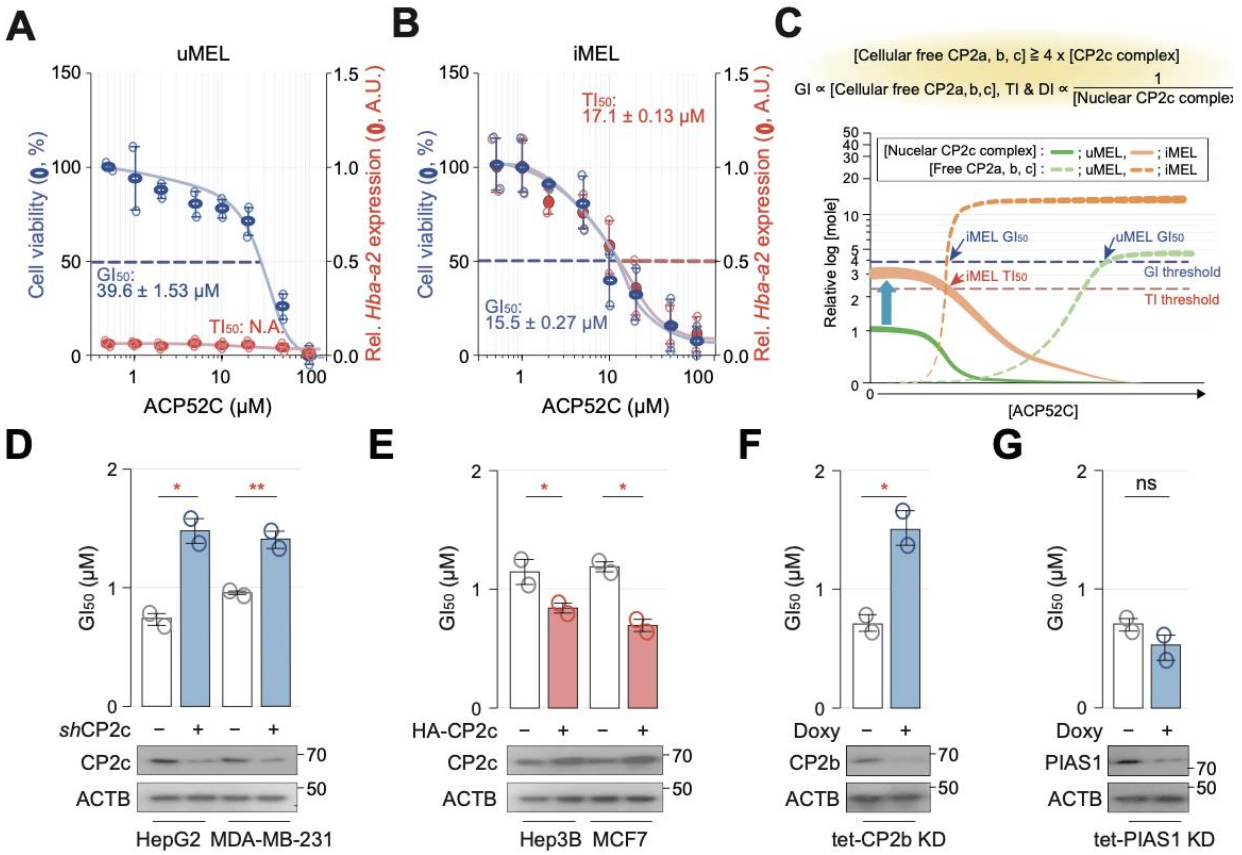


**Figure S13. The relationship between ACP52C-mediated growth inhibition and transcriptional inhibition**

A,B) ACP52C-mediated growth inhibition and transcriptional inhibition of the α-globin gene during MEL cell differentiation in vitro. Cell viability and α-globin mRNA expression in uMEL (A) and iMEL cells (B) at 36 h after ACP52C treatment of various doses. It is note that uMEL cells exhibit marginal α-globin gene expression due to limited CP2c transcriptional complexes, while iMEL cells actively express the α-globin gene with approximately three-fold induction of CP2c and CP2b at the mRNA level during differentiation. Cell viability and relative *Hba-a2* mRNA expression data are presented as means ± SD of two independent biological replicates. $GI_{50}$ and $TI_{50}$ values estimated from two independent biological replicates. C) Schematic explaining the relationship between $GI_{50}$ values and $TI_{50}$ values of the α-globin mRNA expression in uMEL and iMEL cells. D-G) Anticancer activity of ACP52C correlates with cellular concentration of both CP2c and CP2b, but not with PIAS1. Modulation of $GI_{50}$ values in cancer cells by CP2c KD (D) or CP2c OE (E), and in MDA-MB-231 cells by CP2b KD (F) or PIAS1 KD (G), at 96 h after ACP52C treatment. $GI_{50}$ values were estimated from the cell growth inhibition profiles. Duplicated data are expressed as means ± SD. Two-tailed unpaired Student's *t*-tests; *, $P < 0.05$; **, $P < 0.01$; ns, non-significant.

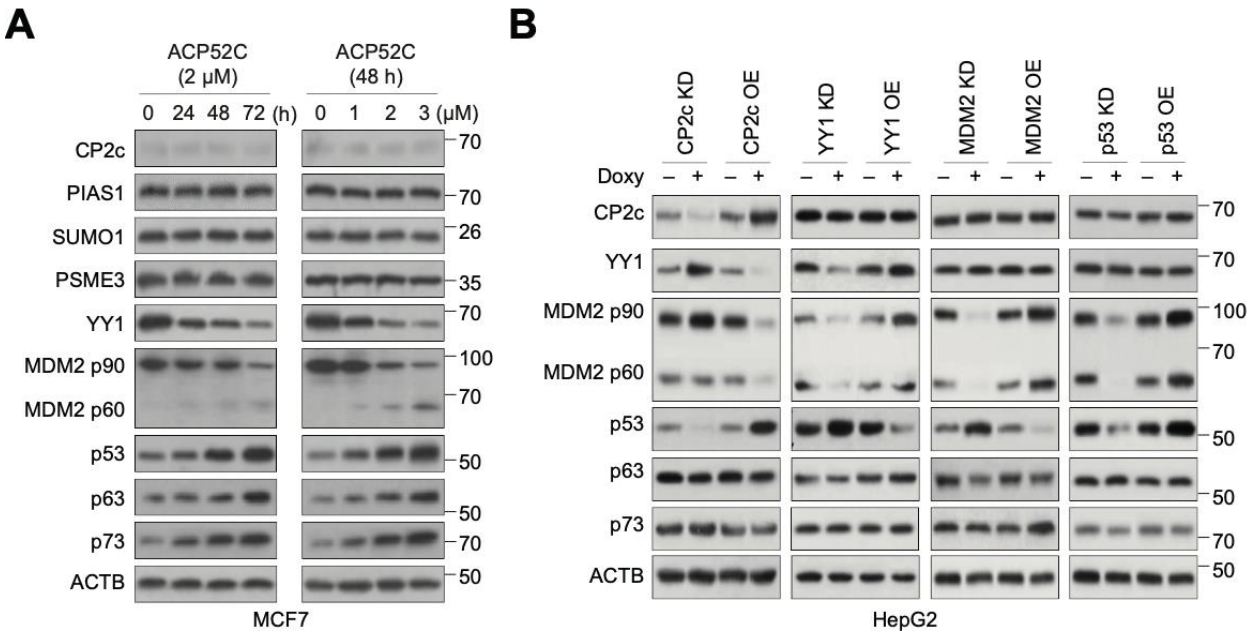


**Figure S14. ACP52C modulates signaling in the CP2c/YY1/MDM2 p90/p53 axis**

A) WBs demonstrating the modulation of proteins in ACP52C-treated MCF7 cells over time (left) and dose (right). B) WBs illustrating the modulation of proteins in HepG2 cells through Tet-inducible KD or OE of CP2c, YY1, MDM2, or p53.

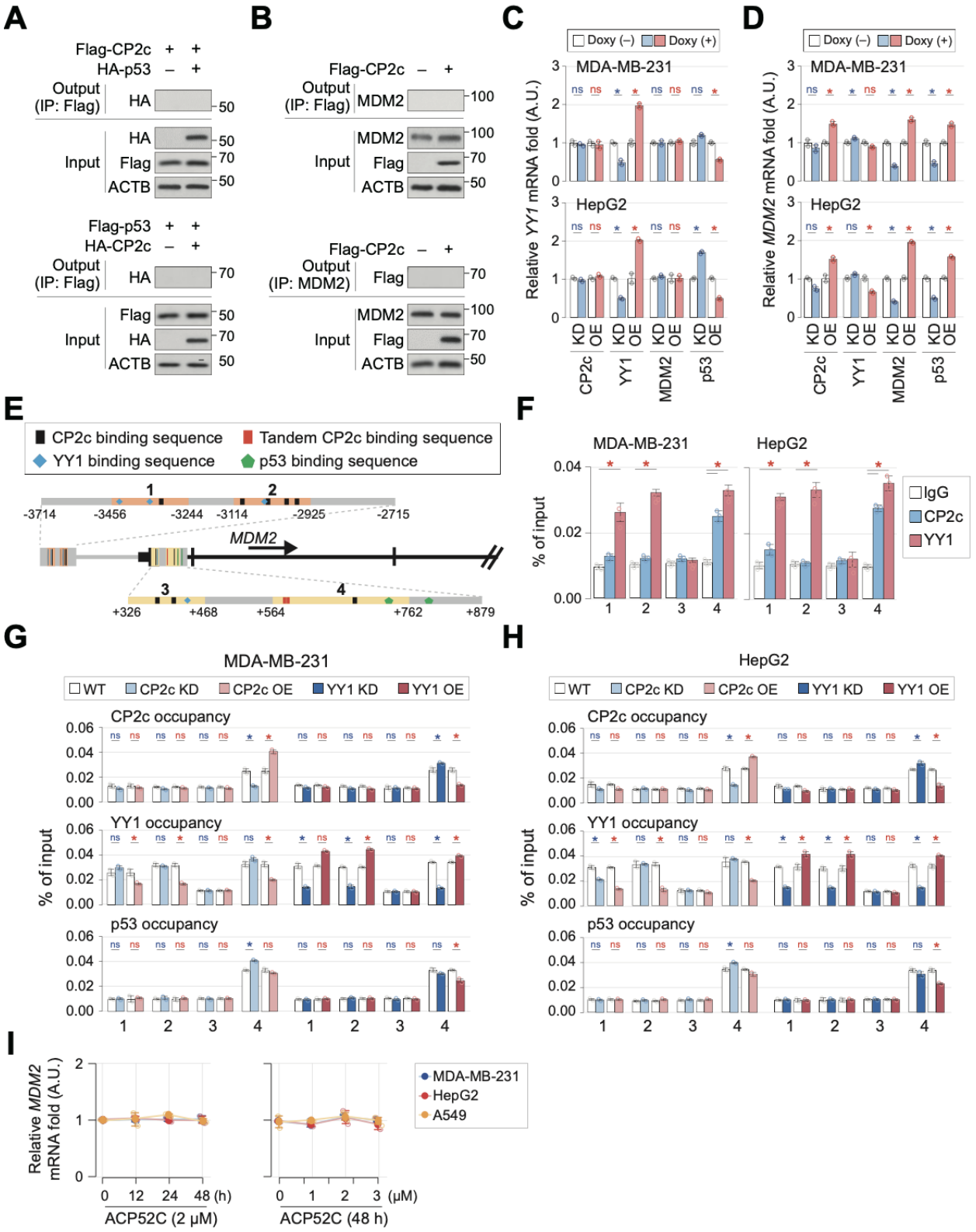


**Figure S15. ACP52C modulates the expression of CP2c/YY1/MDM2 p90/p53 axis proteins in a transcription activity-independent manner**

A,B) Co-IPs demonstrate that CP2c does not directly bind to either p53 (A) or MDM2 p90 (B) in 293T cells. C,D) Transcriptional changes of YY1 (C) and MDM2 p90 (D) were monitored in MDA-MB-231 cells by conditionally modulating the expression of CP2c, YY1, MDM2 p90, or p53. Duplicated data are expressed as means ± SD. Two-tailed unpaired Student's *t*-tests; *, $P < 0.05$; ns, non-significant. E-I) *MDM2* transcription is induced by CP2c but not by ACP52C. (E) Schematic drawing of the *MDM2* gene and its regulatory regions. Regions 1-4 were tested by ChIP-qPCR. Open vertical arrows represent target regions for PCR analyses. (F-H) Factor occupancy tests in the promoter and enhancers of the *MDM2* gene by ChIP-qPCR. Quantification of each factor binding in wildtype cells (F), or by modulation of CP2c and YY1 expression in MDA-MB-231 (G) and HepG2 (H) cells. Duplicated data are expressed as means ± SD. Two-tailed unpaired Student's *t*-tests; *, $P < 0.05$; **, $P < 0.01$; ns, non-significant. (I) *MDM2* transcriptional levels are presented in MDA-MB-231, HepG2, and A549 cells with ACP52C treatment over time. Duplicated data are expressed as means ± SD.

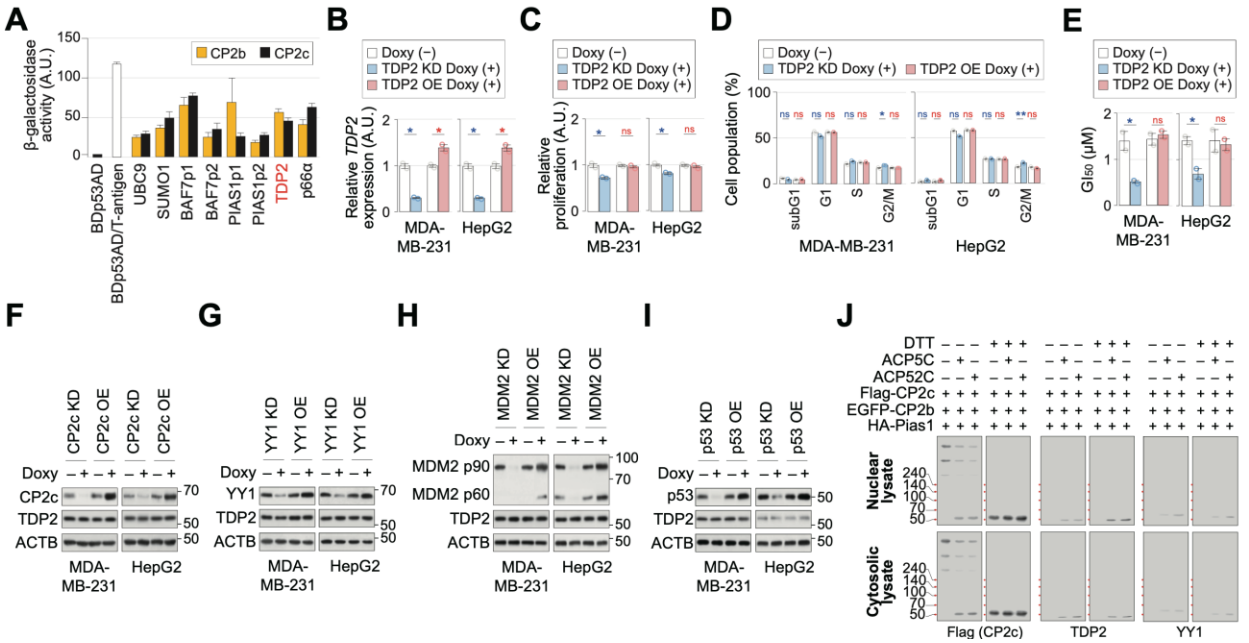


**Figure S16. Identification and characterization of TDP2 as one of CP2c interaction proteins**

A) Identification of TDP2 as one of CP2c-interacting proteins by yeast 2-hybrid. Duplicated data are expressed as means ± SD. B-E) TDP2 KD, but not OE, inhibits cell proliferation and cell cycle progression. (B) RT-qPCR confirms Tet-inducible TDP2 KD and OE in MDA-MB-231 (LM1 line) and HepG2 cells. Graphical presentations of cell proliferation (C) and cell cycle distribution (D) by TDP2 KD or OE. Duplicated data are expressed as means ± SD. Two-tailed unpaired Student's *t*-tests; *, $P < 0.05$; **, $P < 0.01$; ns, non-significant. (E) Modulation of $GI_{50}$ values of ACP52C in cells by TDP2 KD or OE. Duplicated data are expressed as means ± SD. Two-tailed unpaired Student's *t*-tests; *, $P < 0.05$; ns, non-significant. F-I) WBs showing that TDP2 protein is not modulated by CP2c/YY1/MDM2 p90/p53 axis proteins. It is of noting that TDP2 WBs were created after deprobing/reprobing of blots in Figure 4D; Figure S14B, and control immunoblots corresponding to CP2c, YY1, MDM2 p90, p53, and ACTB were the same to those in Figure 4D; Figure S14B, Supporting Information. J) DSP XL-WB demonstrates that TDP2 and YY1 bind to CP2c monomers liberated by ACP52C treatment, but not to CP2c in the complexes.

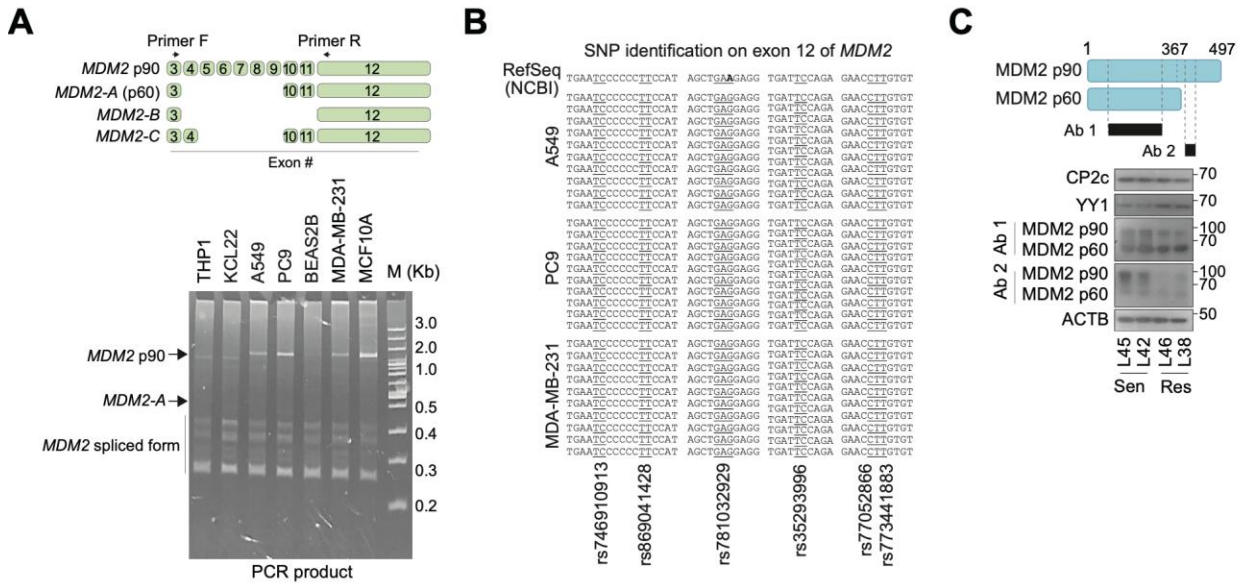


**Figure S17. *MDM2* alternative splicing or SNPs is not involved in the ACP52C resistance**

A) The schematic illustrates a PCR strategy for detecting various known *MDM2* splicing variants (top) and displays the PCR products in various ACP52CGK-sensitive and -resistant cells (bottom). B) Comparisons of SNPs in the *MDM2* exon 12 regions in ACP52CGK-sensitive (MDA-MB-231) and -resistant (PC9 and A549) cells. DNA sequences amplified by genomic PCR from each cell were cloned into the plasmid vector, sequenced, and compared to the RefSeq. C) WBs demonstrate that ACP52C resistance in human liver cancer patient samples is correlated with the expression level of C-terminal truncated MDM2 p60.

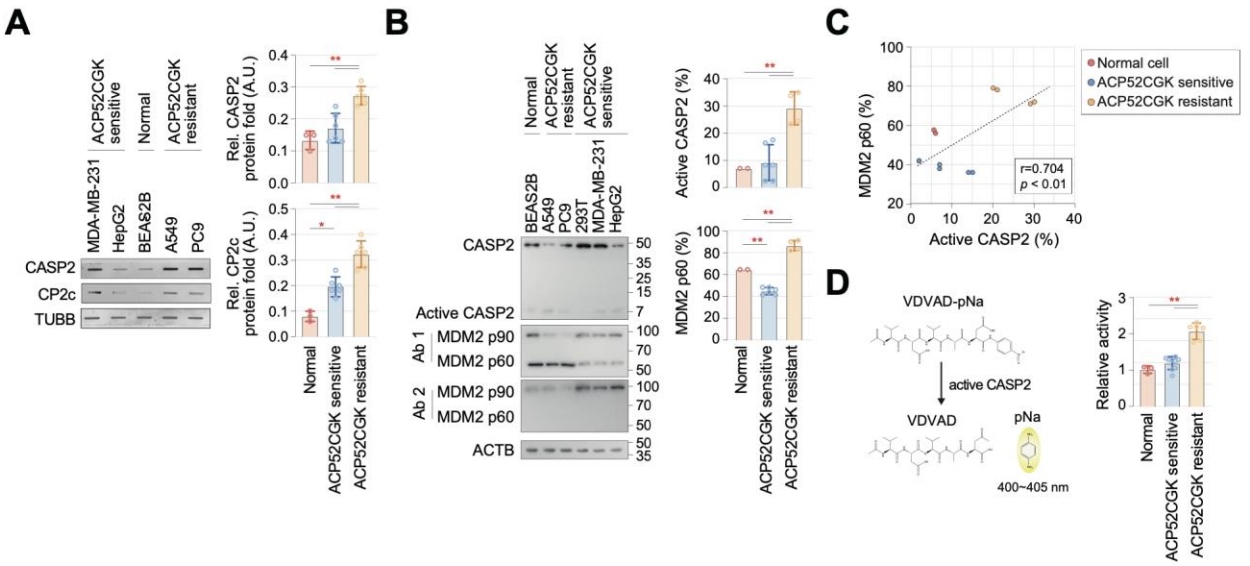


**Figure S18. CASP2-mediated MDM2 p90 cleavage is involved in ACP52CGK resistance in cancer cells**

A) ACP52CGK-resistant cancer cells exhibit significantly higher expression of CASP2 compared to ACP52CGK-sensitive cells. Expressions of CASP2 and CP2c in ACP52CGK-sensitive and -resistant cancer cell lines are accessed using slot blots. Representative slot blots (left) and their relative expression to β-tubulin (right) are shown. Triplicated data are expressed as means ± SD. Two-tailed unpaired Student's *t*-tests; *, $P < 0.05$; **, $P < 0.01$. B) ACP52CGK-resistant cells demonstrate significantly higher CASP2 activity and MDM p60 production when compared to ACP52CGK-sensitive cells. Expressions of CASP2 and MDM2 p90 and p60 in ACP52CGK-sensitive and -resistant cancer cell lines are accessed by WBs. Representative WBs (left) and the quantified fractions of the active CASP2 and the MDM2 p60 (right) are shown. Duplicated data are expressed as means ± SD. Two-tailed unpaired Student's *t*-tests; **, $P < 0.01$. C) The production of MDM2 p60 shows a positive correlation with CASP2 activity in cancer cells according to Pearson's correlation test. D) Experimental validation demonstrates that ACP52CGK-resistant cells have significantly higher cleavage activity of the CASP2-specific substrate compared to ACP52CGK-sensitive cells. Triplicated data are expressed as means ± SD. Two-tailed unpaired Student's *t*-tests; **, $P < 0.01$.

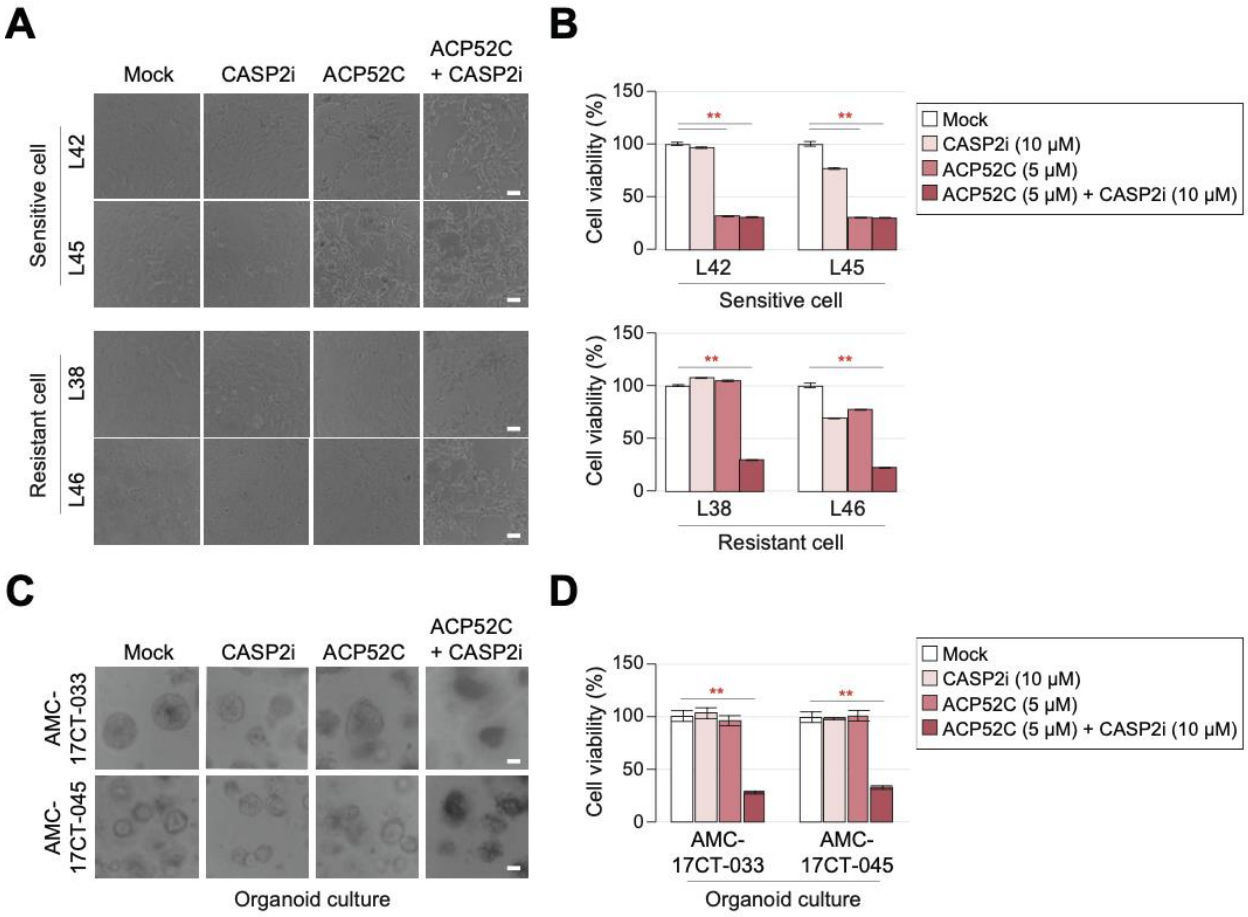


**Figure S19. The combined treatment of ACP52C and the CASP2 inhibitor sensitizes ACP5C2-resistance in human cancers**

A,B) Tests of cell death induction in primary cultured cells derived from human liver cancer patients by treatments of ACP52C alone or in combination with a CASP2 inhibiting peptide. Representative photographs of cells (A) and relative cell viability (B). Duplicated data are expressed as means ± SD. Two-tailed unpaired Student's *t*-tests; **, $P < 0.01$. C,D) Tests of cell death induction in organoids derived from human colon cancer patients by treatments of ACP52C alone or in combination with a CASP2 inhibiting peptide. Representative photographs of organoids (C) and relative cell viability (D). Duplicated data are expressed as means ± SD. Two-tailed unpaired Student's *t*-tests; **, $P < 0.01$.

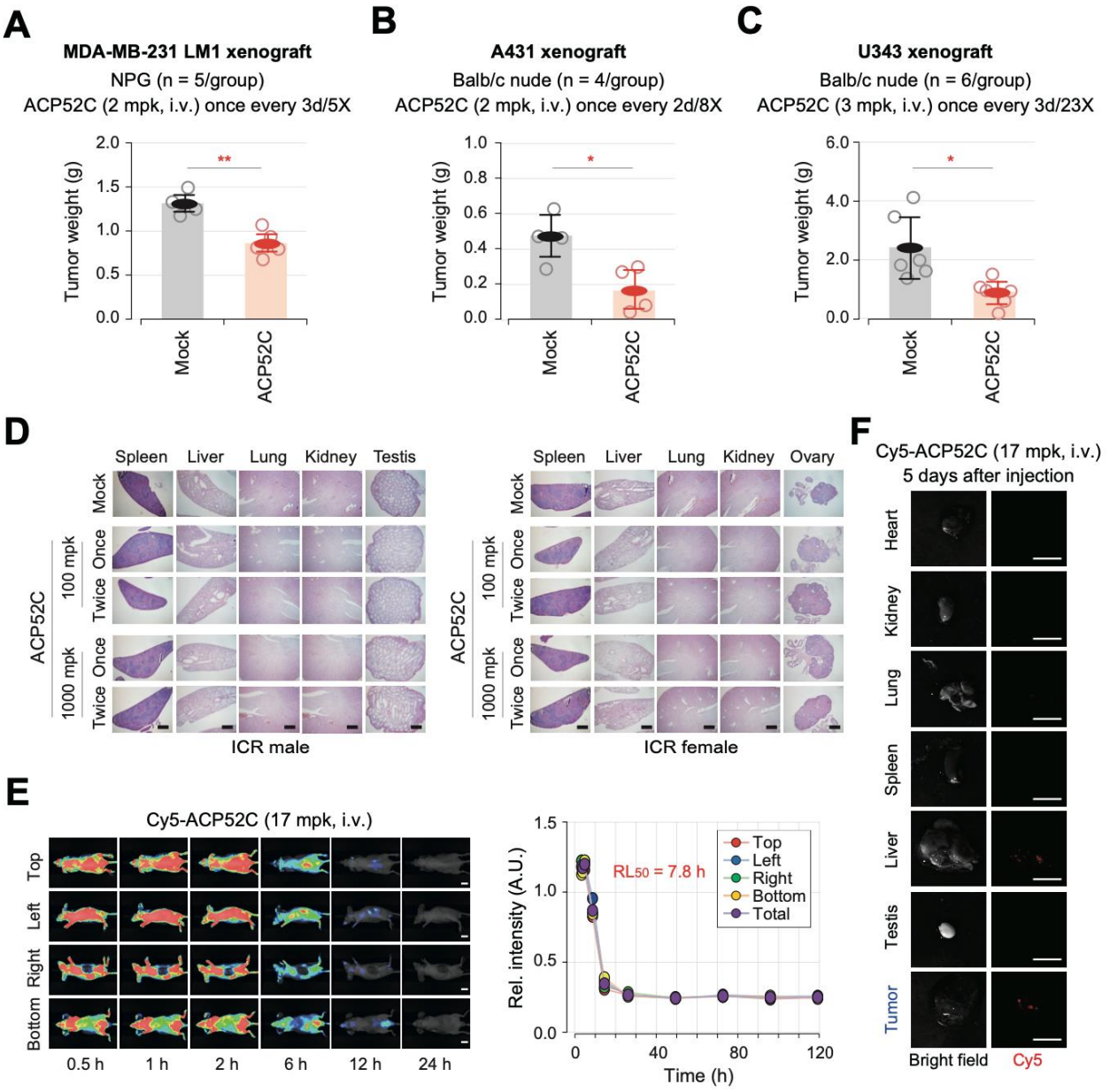


**Figure S20. ACP52C efficacies in vivo**

A-C) Anticancer effects of ACP52C in xenograft model mice. ACP52C reduces tumor weight in MDA-MB-231 LM1 (A), A431 (B), and U343 (C) CDX mice. Data are expressed as means ± SD, and the number of individuals per experimental group is indicated in the figure. Two-tailed unpaired Student's *t*-tests; *, $P < 0.05$; **, $P < 0.01$. D) ACP52C does not show any adverse side effects in the repeated toxicity test in the major organ of normal male and female mice (n = 2/group). The mock group received saline as the vehicle, while the experimental group received injections of ACP52C at doses of 100 mpk or 1000 mpk. "Once" indicates organs collected from mice sacrificed 4 days after a single injection of the drugs, whereas "Twice" refers to organs collected from mice sacrificed 4 days after receiving drug injections twice every 4 days. Scale bar represents 200 μm. E,F) ACP52C exhibits a short residual presence in the body along with effective tumor targeting. (E) Live imaging of Hep3B cell xenograft mice after intravenous administration of Cy5-ACP52C via the tail vein (left). The estimated residual levels of Cy5-ACP52C in the body over time were determined by quantifying the fluorescence intensity of images (right). $RL_{50}$ represents the required time for a 50% retention of fluorescence level. (F) Bright field and fluorescence images of the

major organs and tumor tissue at 5 days after Cy5-ACP52C injection. Scale bar represents 1 cm. It is worth noting that there were no animal deaths related to drug administration in any of the animal studies, although there was one animal death in some treatment groups.

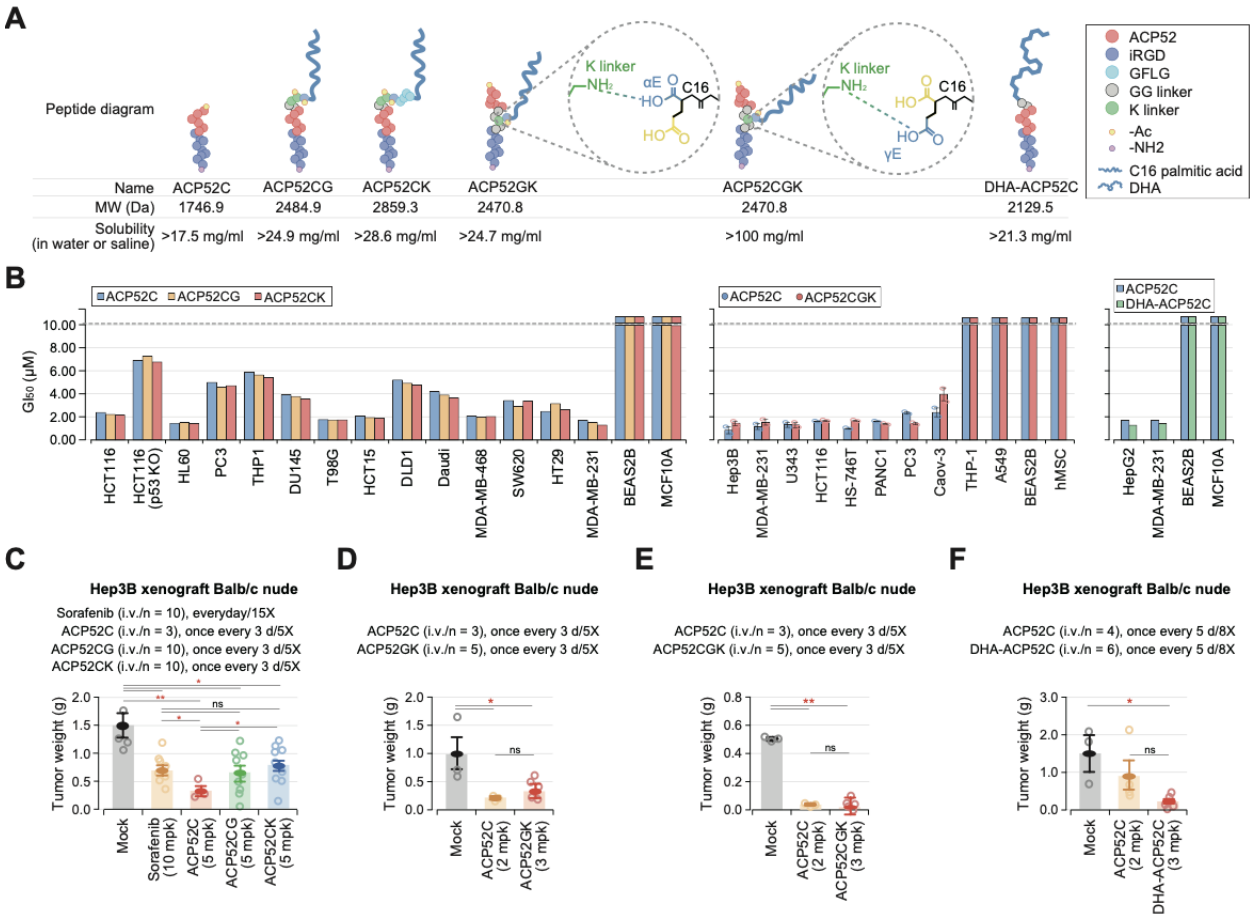


**Figure S21. Anticancer activities of the fatty acid-conjugated derivatives of ACP52C**

A) A schematic representation depicting the structural diagrams, molecular weights, and minimum solubilities (in water or saline) of ACP52C and its derivatives. B) $GI_{50}$ values of ACP52C derivatives in the selected cell lines. C-F) In vivo efficacies of ACP52C derivatives in the Hep3B CDX mice. Tumor weight in the sacrificed mice after completion of drug administration schedule was expressed as means ± SE. ANOVA tests; *, $P < 0.05$; **, $P < 0.01$; ns, non-significant. It is worth noting that there were no animal deaths related to drug administration in any of the animal studies, although there was one animal death in some treatment groups.

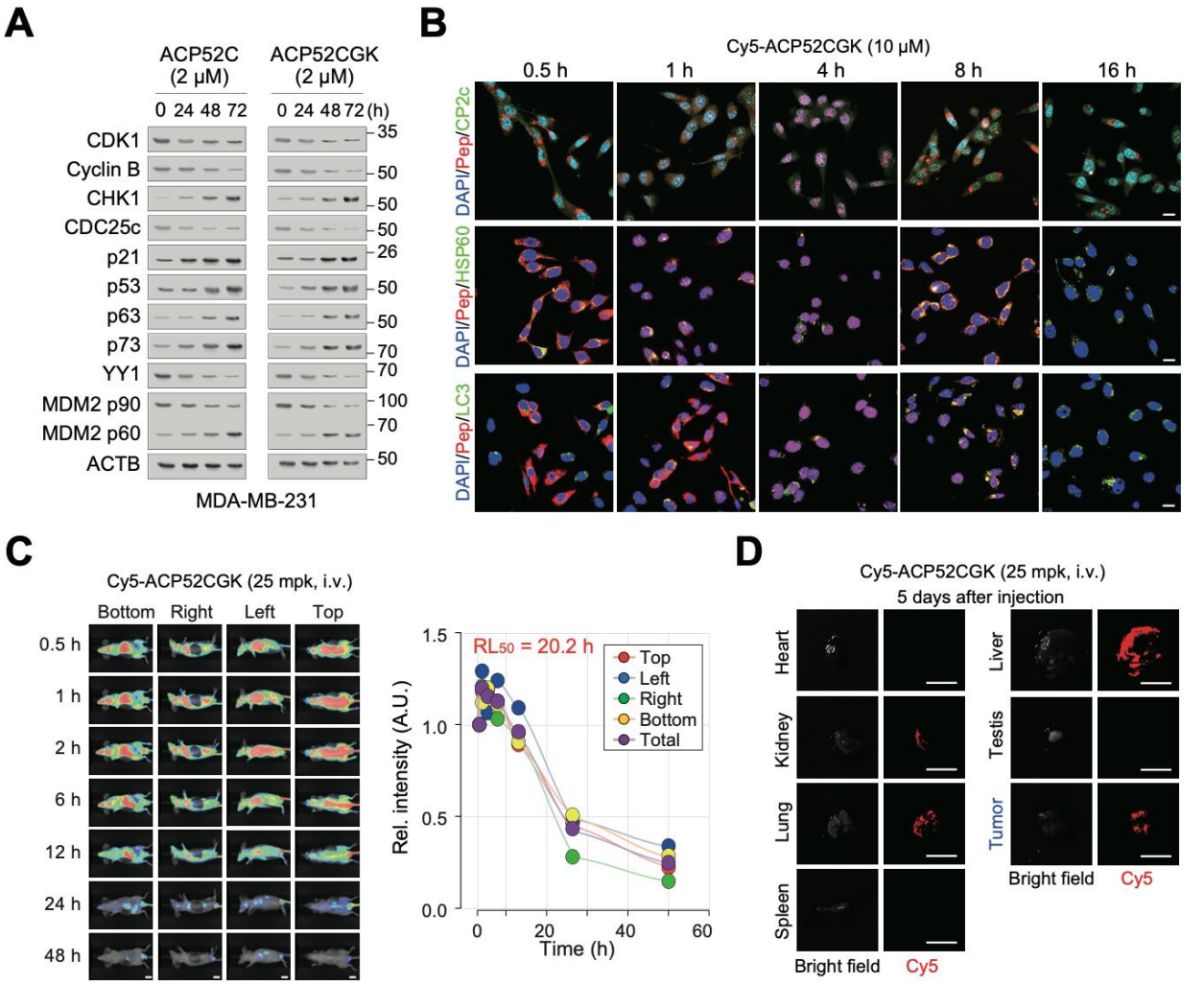


**Figure S22. ACP52CGK shows improved pharmacokinetics compared to ACP52C**

A) WBs show that ACP52CGK retains the same mode-of-action of ACP52C, exhibiting similar effects on markers expression. B) Time-dependent subcellular localization of ACP52CGK. Cy5-ACP52C (10 μM) was supplemented to the culture medium for 30 min to MDA-MB-231 cells, and IF was performed at different time points after replenishing the fresh medium to observe the subcellular localization of ACP52C. Scale bar represents 10 μm. C,D) ACP52CGK shows an improved residual presence in the body with effective tumor targeting. (C) Live imaging of the Hep3B CDX mouse after intravenous injection of Cy5-ACP52CGK via the tail vein (left). The estimated residual levels of Cy5-ACP52C in the body over time were determined by quantifying the fluorescence intensity of images (right). $RL_{50}$ represents the required time for a 50% retention of fluorescence level. (D) Bright field and fluorescence images of the major organs and tumor tissue at 5 days after Cy5-ACP52CGK injection. Scale bar represents 1 cm.

**A**

ACP52CGK (5 mpk, i.v., 48 h)

| PK Parameters | ACP52CGK |
|---|---|
| Dose (mg/kg) | 5 |
| $C_0$ (ng/mL) | 79175 |
| $T_{1/2}$ (h) | 5.26 |
| $Vd_{ss}$ (L/kg) | 0.124 |
| Cl(mL/min/kg) | 0.275 |
| $T_{last}$ (h) | 48 |
| $AUC_{0\text{-}last}$ (ng.h/mL) | 302798 |
| $AUC_{0\text{-}24}$ (ng.h/mL) | 290286 |
| $AUC_{0\text{-}inf}$ (ng.h/mL) | 303344 |
| $MRT_{0\text{-}last}$ (h) | 7.44 |
| $MRT_{0\text{-}inf}$ (h) | 7.53 |
| $AUC_{Extra}$ (%) | 0.180 |
| $AUMC_{Extra}$ (%) | 1.33 |

**B**

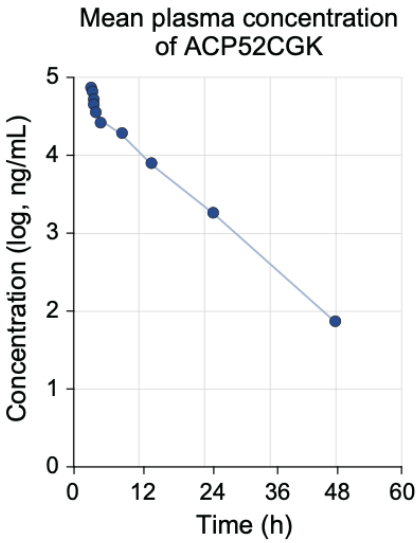


**Figure S23. Pharmacokinetics analysis of ACP52CGK**

A) PK parameters of ACP52CGK in CD-1(ICR) mice, calculated using the noncompartmental analysis model 201 of Phoenix WinNonlin version 6.3. B) Mean plasma concentration of ACP52CGK at 0.033, 0.083, 0.25, 0.5, 1, 2, 6, 12, 24, and 48 h after dosing.

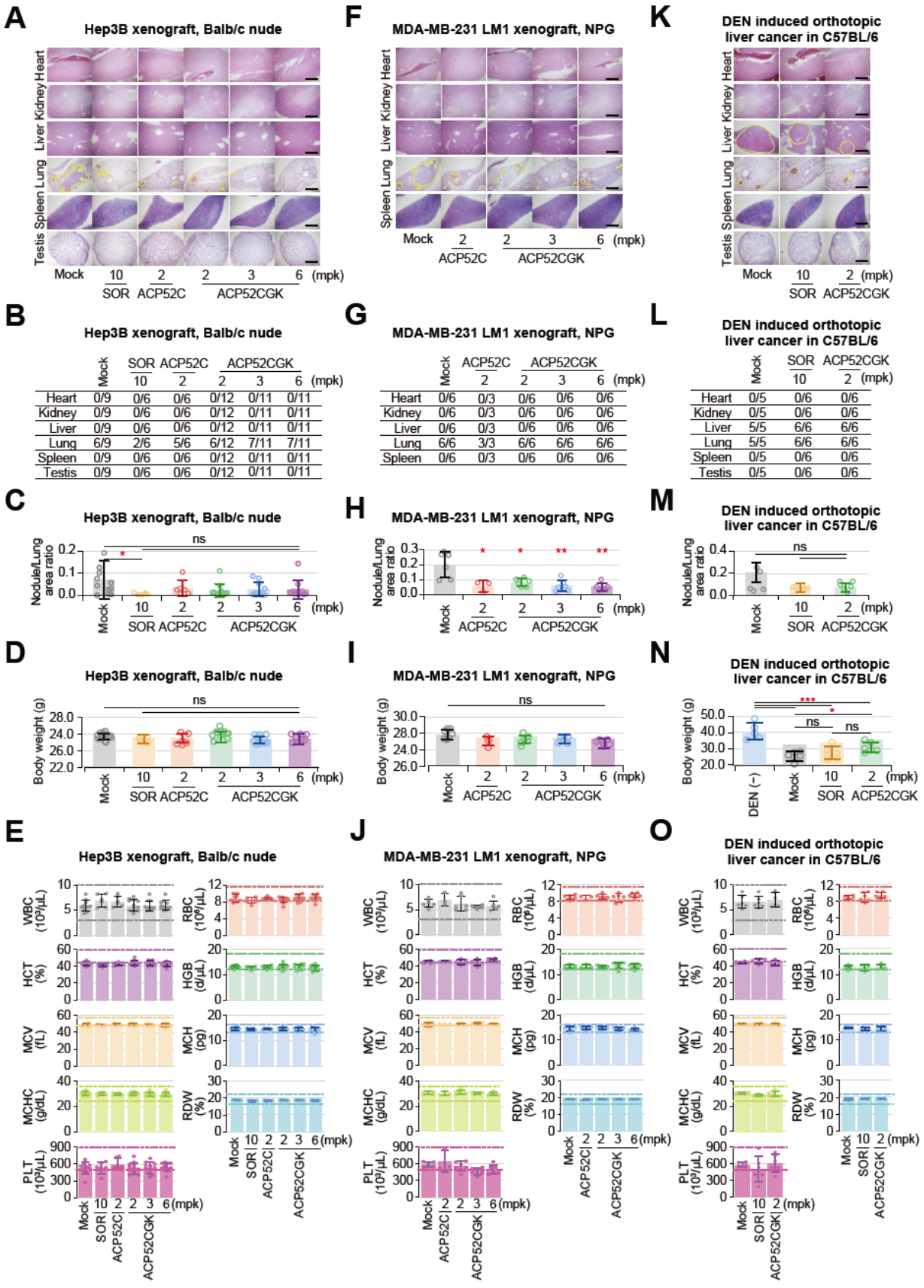
A
Hep3B xenograft, Balb/c nude
Heart
Liver
Kidney
Lung
Spleen
Testis
Mock
10
SOR
2
ACP52C
2
3
6
(mpk)
ACP52CGK
F
MDA-MB-231 LM1 xenograft, NPG
K
DEN induced orthotopic liver cancer in C57BL/6
B
Hep3B xenograft, Balb/c nude
Mock SOR ACP52C ACP52CGK
10 2 2 3 6 (mpk)
Heart 0/9 0/6 0/6 0/12 0/11 0/11
Kidney 0/9 0/6 0/6 0/12 0/11 0/11
Liver 0/9 0/6 0/6 0/12 0/11 0/11
Lung 6/9 2/6 5/6 6/12 7/11 7/11
Spleen 0/9 0/6 0/6 0/12 0/11 0/11
Testis 0/9 0/6 0/6 0/12 0/11 0/11
G
MDA-MB-231 LM1 xenograft, NPG
Mock ACP52C ACP52CGK
2 2 3 6 (mpk)
Heart 0/6 0/3 0/6 0/6 0/6
Kidney 0/6 0/3 0/6 0/6 0/6
Liver 0/6 0/3 0/6 0/6 0/6
Lung 6/6 3/3 6/6 6/6 6/6
Spleen 0/6 0/3 0/6 0/6 0/6
L
DEN induced orthotopic liver cancer in C57BL/6
Mock SOR ACP52CGK
10 2 (mpk)
Heart 0/5 0/6 0/6
Kidney 0/5 0/6 0/6
Liver 5/5 6/6 6/6
Lung 5/5 6/6 6/6
Spleen 0/5 0/6 0/6
Testis 0/5 0/6 0/6
C
Hep3B xenograft, Balb/c nude
Nodule/Lung area ratio
ns
*
Mock
10
SOR
2
ACP52C
2
3
6
(mpk)
ACP52CGK
H
MDA-MB-231 LM1 xenograft, NPG
*
*
**
**
M
DEN induced orthotopic liver cancer in C57BL/6
D
Hep3B xenograft, Balb/c nude
Body weight (g)
ns
I
MDA-MB-231 LM1 xenograft, NPG
N
DEN induced orthotopic liver cancer in C57BL/6
***
*
ns
ns
DEN (-)
E
Hep3B xenograft, Balb/c nude
WBC (10³/μL)
RBC (10⁶/μL)
HCT (%)
HGB (d/μL)
MCV (fL)
MCH (pg)
MCHC (g/dL)
RDW (%)
PLT (10³/μL)
J
MDA-MB-231 LM1 xenograft, NPG
O
DEN induced orthotopic liver cancer in C57BL/6

**Figure S24. Evaluation of ACP52CGK on metastasis and side effects in three different mouse cancer models**

A-O) Hep3B CDX (A-E) and MDA-MB-231 LM1 CDX (F-J) mouse cancer models, as well as the DEN-induced orthotopic liver cancer model (K-O). The number of individuals per experimental group is consistent in the xenograft model corresponding to Figure 7. Representative images of H&E-stained tissue sections from major organs harvested from xenograft mice upon completion of the drug administration (A, F, and K). Histological scoring of tumor-bearing mice/total mice (B, G, and L) and the nodule area/lung area (C, H, and M) in the H&E-stained major organs of tumor-bearing mice. Body weights of mice (D, I, and N) and CBC analysis of each treated group of mice (E, J, and O) at the experiment's conclusion. Data are expressed as means ± SD. The two dotted lines in each graph represent the high and low limits of values in normal mice. Data are expressed as means ± SD. ANOVA tests;*, $P < 0.05$; **, $P < 0.01$; ***, $P < 0.001$; ns, non-significant. Scale bars in (A, F, and K), 500 μm. WBC, white blood cell count; RBC, red blood cell count; HCT, hematocrit; HGB, hemoglobin; MCV, mean corpuscular volume; MCH, mean corpuscular hemoglobin; MCHC, mean corpuscular hemoglobin concentration; RDW, red cell distribution width; PLT, platelet count. It is worth noting that there were no animal deaths related to drug administration in any of the animal studies.

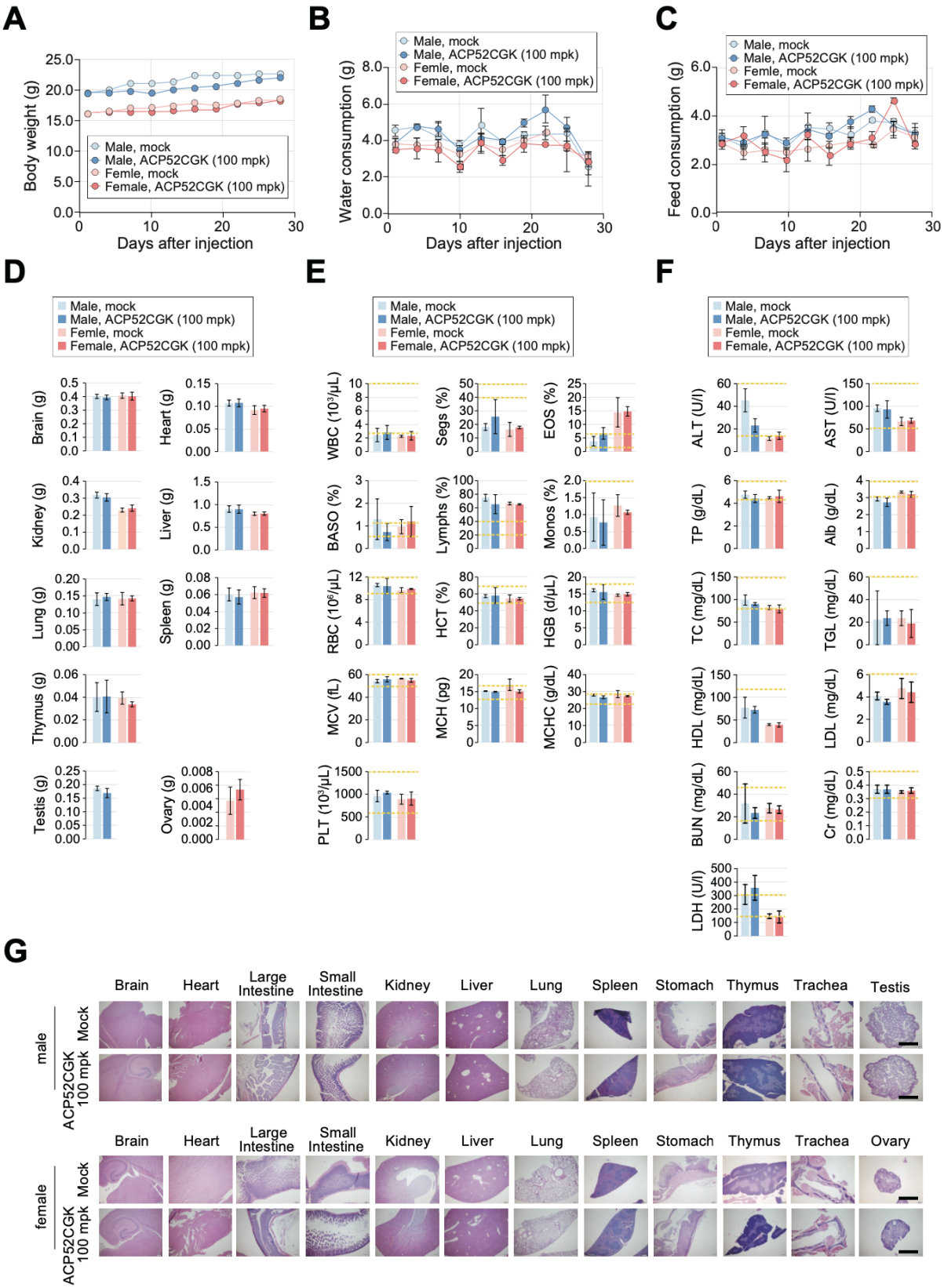


**Figure S25. ACP52CGK does not show any adverse side effects in the repeated toxicity test in normal male and female mice**

Repeated toxicity test of ACP52CGK were analyzed in ICR mice by intravenous injection of 100 mpk of ACP52CGK daily for 4 weeks (n = 6/group). A-C) Body weight (A), water consumption (B), and food consumption (C) were measured once every 3 days after injection. D-F) Major organ weight (D), CBC (E), and blood chemistry (F) were measured after sacrifice. Data are expressed as means ± SD in (B-F). G) ACP52CGK does not show any adverse side effects in the repeated toxicity test in normal male and female mice. Scale bar represents 200 μm. It is worth noting that there were no animal deaths related to drug administration in any of the animal studies.

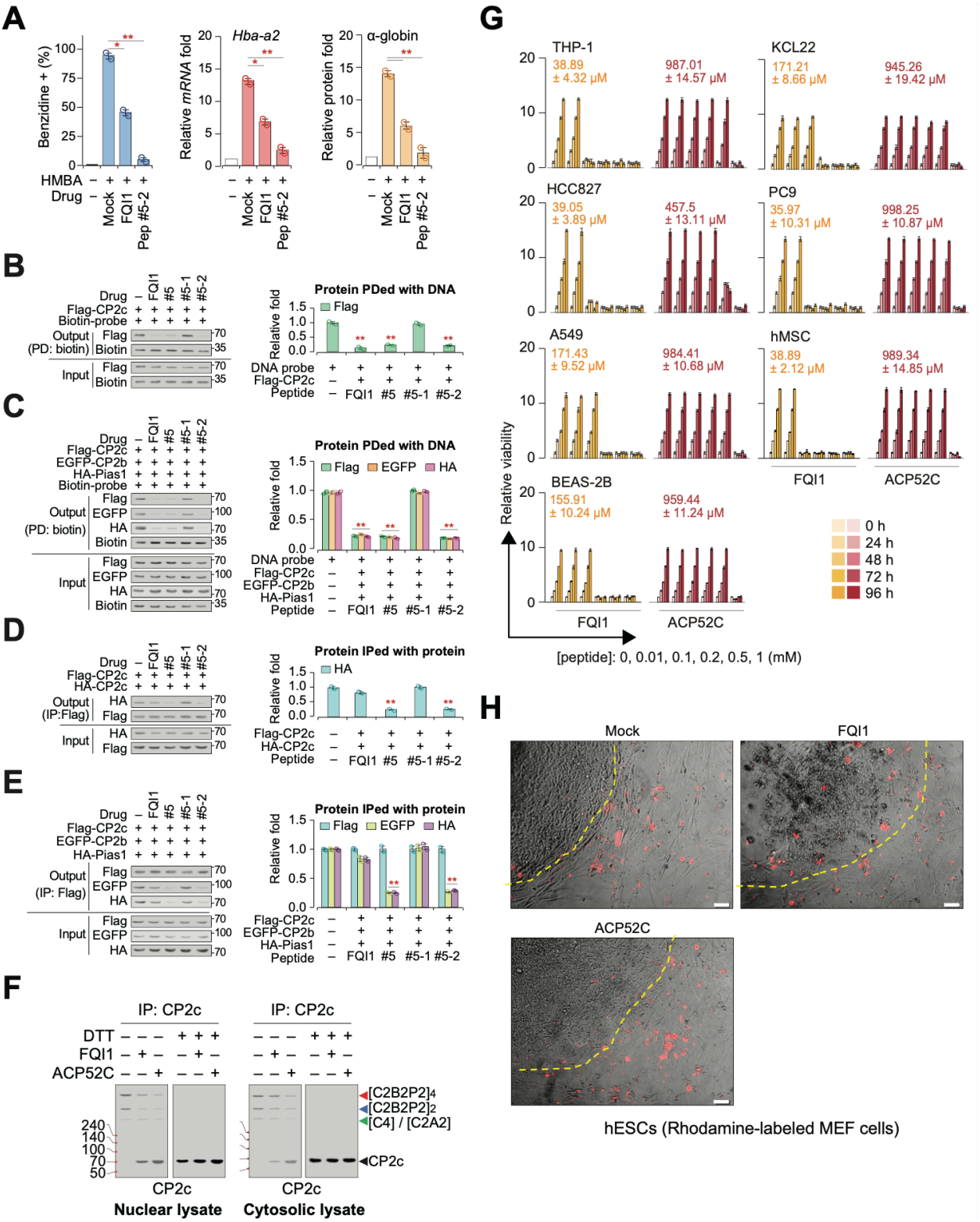


**Figure S26. ACP52C is superior to another CP2c-targeting small molecule, FQI1, in terms of efficacy and safety at the level of cultured cells**

A) Pep #5-2C (ACP52C) efficiently inhibits functional hemoglobin synthesis (left), and *Hba-a2* globin gene expression at both mRNA (middle) and protein (right) levels in iMEL cells, surpassing the

performance of FQI1. Two micromoles of each Pep #5-2C and FQI1 were added to the cell culture for 2 days. Fractions of benzidine-positive stained cells were counted in MEL cells (n > 100 cells/group) treated with HMBA for 2 days. *Hba-a2* gene expression at mRNA and protein levels were estimated by RT-qPCR and WB, respectively. Data are presented as means ± SD of two independent biological replicates. ANOVA test; * $P < 0.05$, ** $P < 0.01$. B,C) FQI1 efficiently inhibits the DNA binding ability of CP2c complexes similar performance of Pep #5 or Pep #5-2. DNA-pull down assays for the [C4] complex (B) and the CBP complexes (C). Data are presented as means ± SD of two independent biological replicates. Two-tailed unpaired Student's *t*-tests; ** $P < 0.01$. D,E) Pep #5 and Pep #5-2 efficiently inhibits the CP2c complex formation by itself, surpassing the performance of FQI1. Co-IP assays for the [C4] complex (D) and the CBP complexes (E). Data are presented as means ± SD of two independent biological replicates. Student's *t*-tests; ** $P < 0.01$. F) DSP XL-WB demonstrates that ACP52C disrupt CP2c complexes more effectively than FQI1. G) Cell growth inhibition plots and $GI_{50}$ values of FQI1 and ACP52C in various cancer cell lines and normal cells over peptide dose. $GI_{50}$ values estimated from two independent biological replicates. H) Representative images showing that FQI1 induces cell death in hESC cells, whereas ACP52C does not. hESCs were cultured on the Rhodamine-labeled MEF cells. Ten micromoles of each ACP52C and FQI1 were added to the cell culture for 3 days before capturing images of cultures.

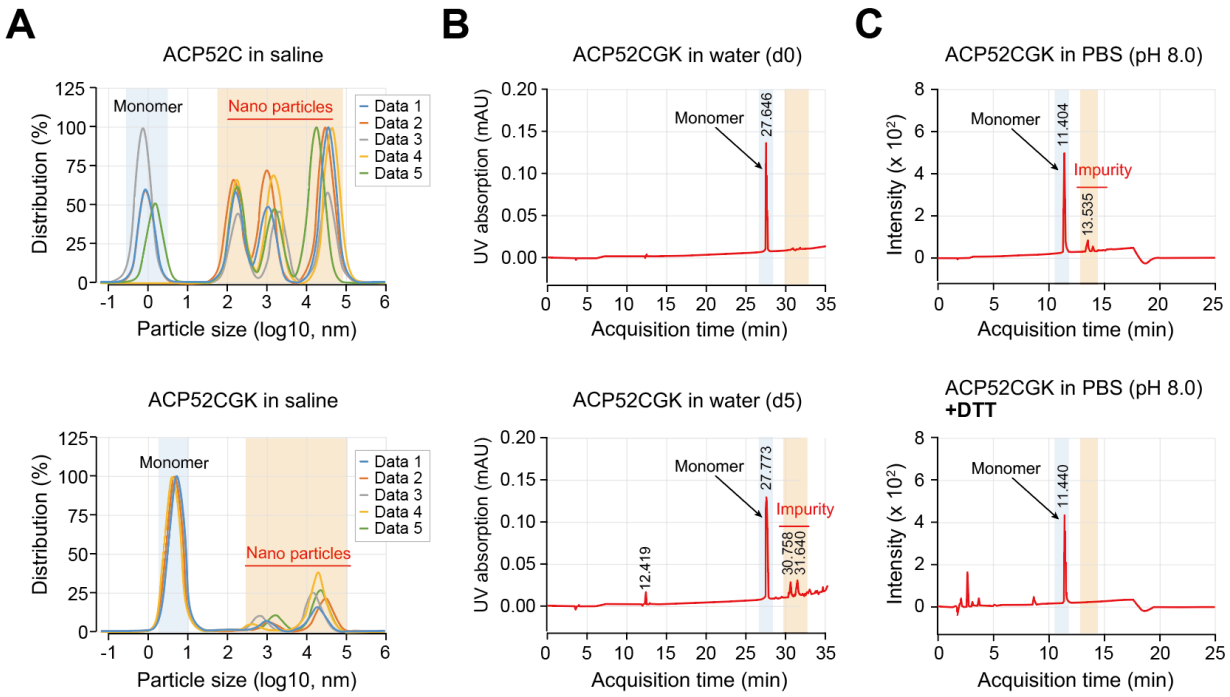


**Figure S27. Physicochemical analysis confirms stability and purity issues of ACP52CGK due to inter-strand disulfide bond formation.**

A) Dynamic Light Scattering (DLS) analysis was conducted on both ACP52C and ACP52CGK in a saline solution to assess their nanoparticle formation characteristics. The data are presented with five independent measurements to ensure reproducibility. B) The results of HPLC analysis demonstrate the presence of larger particles (i.e., impurities) in ACP52CGK in water over a period of 5 days. C) LC-MS analysis demonstrates the elimination of impurity patterns in ACP52CGK through the use of DTT treatment.

**Table S1.**
Information of cell lines

| Cell line | Source | RRID number | Cat number | Media & supplement |
|---|---|---|---|---|
| Daudi | blood (B lymphoblast) | RRID:CVCL_0008 | ATCC no. CCL-213 | RPMI, 10%FBS, P/S |
| HEL | blood (erythroblast) | RRID:CVCL_0001 | ATCC no. TIB-180 | RPMI, 10%FBS, P/S |
| THP1 | blood (monocyte) | RRID:CVCL_0006 | ATCC no. TIB-202 | RPMI, 10%FBS, P/S |
| HL60 | blood (promyeloblast) | RRID:CVCL_0002 | ATCC no. CCL-240 | RPMI, 10%FBS, P/S |
| CCRF-CEM | blood (T lymphoblast) | RRID:CVCL_0007 | ATCC no. CCL-119 | RPMI, 10%FBS, P/S |
| Molt4 | blood (T lymphoblast) | RRID:CVCL_0013 | ATCC no. CRL-1582 | RPMI, 10%FBS, P/S |
| Jurkat | blood (T lymphocyte) | RRID:CVCL_0065 | ATCC no. TIB-152 | RPMI, 10%FBS, P/S |
| primary T cell | Blood (T lymphocyte) | | | RPMI, 10%FBS, P/S |
| K562 | bone marrow | RRID:CVCL_0004 | ATCC no. CCL-243 | RPMI, 10%FBS, P/S |
| KCL22 | bone marrow | RRID:CVCL_2091 | ATCC no. CRL-3350 | RPMI, 10%FBS, P/S |
| hCD34+ | bone marrow derived progenitor cells | | | IMDM, 100 ng/ml SCF, 50 ng/ml TPO, supplement |
| U87MG | brain | RRID:CVCL_0022 | ATCC no. HTB-14 | DMEM, 10%FBS, P/S |
| T98G | brain | RRID:CVCL_0556 | ATCC no. CRL-1690 | RPMI, 10%FBS, P/S |
| U251 | brain | RRID:CVCL_0021 | ECACC no. 0861901 | RPMI, 10%FBS, P/S |
| U373MG(= U251) | brain | RRID:CVCL_2818 | ATCC no. HTB-17, | RPMI, 10%FBS, P/S |
| U343 | brain | RRID:CVCL_4773 | | DMEM, 10%FBS, P/S |
| MCF7 | breast | RRID:CVCL_0031 | ATCC no. HTB-22 | DMEM, 10%FBS, P/S |
| MDA-MB-231 | breast | RRID:CVCL_0062 | ATCC no. HTB-26 | DMEM, 10%FBS, P/S |
| MCF10A | breast | RRID:CVCL_0598 | ATCC no. CRL-10317 | DMEM/F12, 5% HS, 400 ng/ml hydrocortisone, 100 ng/ml cholera toxin, 10 µg/ml insulin, 20 ng/ml EGF, P/S |
| MDA-MB-468 | breast | RRID:CVCL_0419 | ATCC no. HTB-132 | RPMI, 10%FBS, P/S |
| SK-BR-3 | breast | RRID:CVCL_0033 | ATCC no. HTB-30 | RPMI, 10%FBS, P/S |
| HeLa | cervix | RRID:CVCL_0030 | ATCC no. CCL-2 | DMEM, 10%FBS, P/S |
| SW620 | colon | RRID:CVCL_0547 | ATCC no. CCL-227 | DMEM, 10%FBS, P/S |
| SW480 | colon | RRID:CVCL_0546 | ATCC no. CCL-228 | DMEM, 10%FBS, P/S |
| RKO | colon | RRID:CVCL_0504 | ATCC no. CRL-2577 | DMEM, 10%FBS, P/S |
| KM12-SM | colon | RRID:CVCL_9548 | | DMEM, 10%FBS, P/S |
| DLD1 | colon | RRID:CVCL_0248 | ATCC no. CCL-221 | RPMI, 10%FBS, P/S |
| Colo205 | colon | RRID:CVCL_0218 | ATCC no. CCL-222 | RPMI, 10%FBS, P/S |
| HCT15 | colon | RRID:CVCL_0292 | ATCC no. CCL-225 | RPMI, 10%FBS, P/S |
| HCT116 (p53 WT) | colon | RRID:CVCL_0291 | ATCC no. CCL-247 | RPMI, 10%FBS, P/S |
| HT29 | colon | RRID:CVCL_0320 | ATCC no. HTB-38 | RPMI, 10%FBS, P/S |
| HCT116 (p53 null) | colon | RRID:CVCL_HD97 | | RPMI, 10%FBS, P/S |
| P-MEF | embryonic fibroblast | RRID:CVCL_9115 | SCRC-1008 | DMEM/F12, 20% serum, 0.1 mM NEAA, 0.1 mM ME, 4 ng/ml bFGF, P/S |
| hESC | human embryo | RRID:CVCL_9262 | US NIH no Miz-hES1 | DMEM/F12, 20% serum, 0.1 mM NEAA, 0.1 mM ME, 4 ng/ml bFGF, P/S |
| 293T | kidney | RRID:CVCL_0063 | ATCC no. CRL-3216 | DMEM, 10%FBS, P/S |
| Hep3B | liver | RRID:CVCL_0326 | ATCC no. HB-8064 | DMEM, 10%FBS, P/S |
| HepG2 | liver | RRID:CVCL_0027 | ATCC no. HB-8065 | DMEM, 10%FBS, P/S |
| SK-Hep1 | liver | RRID:CVCL_0525 | ATCC no. HTB-52 | DMEM, 10%FBS, P/S |
| Huh7 | liver | RRID:CVCL_0336 | JCRB no. 0403 | DMEM, 10%FBS, P/S |
| HepT1 | liver | RRID:CVCL_G003 | | DMEM, 10%FBS, P/S |
| Hep3B Fluc | liver | | ATCC no. HB-8064 | DMEM, 10%FBS, P/S |
| SNU387 | liver | RRID:CVCL_0250 | ATCC no. CRL-2237 | RPMI, 10%FBS, P/S |
| SNU423 | liver | RRID:CVCL_0336 | ATCC no. CRL-2238 | RPMI, 10%FBS, P/S |
| SNU354 | liver | RRID:CVCL_3947 | KCLB no. 00354 | RPMI, 10%FBS, P/S |
| SNU368 | liver | RRID:CVCL_3948 | KCLB no. 00368 | RPMI, 10%FBS, P/S |
| A549 | lung | RRID:CVCL_0023 | ATCC no. CCL-185 | RPMI, 10%FBS, P/S |
| HCC827 | lung | RRID:CVCL_2063 | ATCC no. CRL-2868 | RPMI, 10%FBS, P/S |
| H1975 | lung | RRID:CVCL_1511 | ATCC no. CRL-5908 | RPMI, 10%FBS, P/S |
| BEAS-2B | lung | RRID:CVCL_0168 | ATCC no. CRL-9609 | RPMI, 10%FBS, P/S |
| NCI-H820 | lung | RRID:CVCL_1592 | ATCC no. HTB-181 | RPMI, 10%FBS, P/S |
| HCC827GR | lung | RRID:CVCL_V620 | | RPMI, 10%FBS, P/S |
| HCC827GRKU | lung | | | RPMI, 10%FBS, P/S |
| PC9 | lung | RRID:CVCL_B260 | | RPMI, 10%FBS, P/S |

| | | | | |
|---|---|---|---|---|
| PC9GR | lung | | | RPMI, 10%FBS, P/S |
| H1299 | lung | RRID:CVCL_0060 | ATCC no. CRL-5803 | RPMI, 10%FBS, P/S |
| H2009 | lung | RRID:CVCL_1514 | ATCC no. CRL-5911 | RPMI, 10%FBS, P/S |
| H23 | lung | RRID:CVCL_1547 | ATCC no. CRL-5800 | RPMI, 10%FBS, P/S |
| H358 | lung | RRID:CVCL_1559 | ATCC no. CRL-5807 | RPMI, 10%FBS, P/S |
| H920 | lung | RRID:CVCL_1599 | ATCC no. CRL-5850 | RPMI, 10%FBS, P/S |
| U937 | lymphoma | RRID:CVCL_0007 | ATCC no. CRL-1593.2 | RPMI, 10%FBS, P/S |
| MEL_DS19 | murine blood | RRID:CVCL_2111 | | DMEM, 10%FBS, P/S |
| Caov-3 | ovary | RRID:CVCL_0201 | ATCC no. HTB-75 | DMEM, 10%FBS, P/S |
| SK-OV-3 | ovary | RRID:CVCL_0532 | ATCC no. HTB-77 | RPMI, 10%FBS, P/S |
| MIA-PACA-2 | pancreas | RRID:CVCL_04428 | ATCC no. CRL-1420 | DMEM, 10%FBS, P/S |
| PANC1 | pancreas | RRID:CVCL_0480 | ATCC no. CRL-1469 | DMEM, 10%FBS, P/S |
| DU145 | prostate | RRID:CVCL_0105 | ATCC no. HTB-81 | DMEM, 10%FBS, P/S |
| PC3 | prostate | RRID:CVCL_0035 | ATCC no. CRL-1435 | RPMI, 10%FBS, P/S |
| NLCaP | prostate | RRID:CVCL_0395 | ATCC no. CRL-1740 | RPMI, 10%FBS, P/S |
| A431 | skin | RRID:CVCL_0037 | ATCC no. CRL-1555 | RPMI, 10%FBS, P/S |
| HS-746T | stomach | RRID:CVCL_0333 | ATCC no. HTB-135 | DMEM, 10%FBS, P/S |
| MKN45 | stomach | RRID:CVCL_0434 | | RPMI, 10%FBS, P/S |
| hMSC (LT18) | thigh | | | DMEM-LG, 10%FBS, P/S |
| Breast cancer patient B3 | breast | | | EpiX media |
| Colon cancer patient AMC-17CT-033 | colon | | | Organoid media |
| Colon cancer patient AMC-17CT-045 | colon | | | Organoid media |
| Liver cancer patient L38 | liver | | | EpiX media |
| Liver cancer patient L38 | liver | | | EpiX media |
| Liver cancer patient L42 | liver | | | EpiX media |
| Liver cancer patient L45 | liver | | | EpiX media |
| Liver cancer patient L46 | liver | | | EpiX media |

RRID, Research Resource Identifiers; ATCC, American type culture collection; ECACC, European collection of authenticated cell cultures; SCRC, stem cell research center; JCRB, Japanese collection of research bioresources cell bank; KCLB, Korea cell line bank. EpiX media, KSFM, 50 µg/mL BPE, 5 ng/mL hEGF, 1 µM A83-01, 5 µM Y27632, 3 µM isoproterenol; Organoid media, DMEM/F12, 10 mM HEPES, 1% GlutaMax-1, 100 µg/mL Primocin, 2% B27 supplement, 1% N2 supplement, 1 mM n-Acetyl-L-cysteine, 10 mM nicotinamide, 500 nM A83-01, 50 ng/mL hEGF, 10 nM gastrin1, 10 µM Y27632, P/S

**Table S2.**
Oligonucleotide list

| name | sequence |
|---|---|
| for plasmid construction | |
| hp53_F_MluI | GTT TAA ACA TGG AGG AGC CGC AGT CAG A |
| hp53_R_NdeI | CAC ATA TGT CAG TCT GAG TCA GGC CCT |
| hMDM2_F_PmeI | CGT TTA AAC ATG GTG AGG AGC AGG CA |
| hMDM2_R_SpeI | CCA CTA GTC TAG GGG AAA TAA GTT AG |
| hYY1_F_PmeI | GTT TAA ACA TGG CCT CGG GCG ACA CC |
| hYY1_R_SpeI | GCA CTA GTT CAC TGG TTG TTT TTG GC |
| mCP2c_F_NotI | GCG GCC GCA TGG CCT GGG CTC TGA AG |
| mCP2c_R_NotI | GCG GCC GCC TTG AGA ATG ACA TGA TA |
| *sh*hp53_F | GAT CCC CAC CAT CCA CTA CAA CTA CAT TCA AGA GAT GTA GTT GTA GTG GAT GGT TTT TTA |
| *sh*hp53_R | AGC TTA AAA AAC CAT CCA CTA CAA CTA CAT CTC TTG AAT GTA GTT GTA GTG GAT GGT GGG |
| *sh*hMDM2_F | GAT CCC CAG GAA TTT AGA CAA CCT GAT TCA AGA GAT CAG GTT GTC TAA ATT CCT TTT TTA |
| *sh*hMDM2_R | AGC TTA AAA AAG GAA TTT AGA CAA CCT GAT CTC TTG AAT CAG GTT GTC TAA ATT CCT GGG |
| *sh*hYY1_F | GAT CCC CCG AAT GCT AGA CAA TAG GAT TCA AGA GAT CCT ATT GTC TAG CAT TCG TTT TTA |
| *sh*hYY1_R | AGC TTA AAA ACG AAT GCT AGA CAA TAG GAT CTC TTG AAT CCT ATT GTC TAG CAT TCG GGG |
| *sh*hCP2c_F | GAT CCC CCT AGA ATG AAG CCA AGA AAT TCA AGA GAT TTC TTG GCT TCA TTC TAG TTT TTG GAA A |
| *sh*hCP2c_R | AGC TTT TCC AAA AAC TAG AAT GAA GCC AAG AAA TCT CTT GAA TTT CTT GGC TTC ATT CTA GGG G |
| *sh*hPIAS1_F | GAT CCC CCA TTC CAC AAC TCA CTT ACT TCA AGA GAG TAA GTG AGT TGT GGA ATG TTT TTA |
| *sh*hPIAS1_R | AGC TTA AAA ACA TTC CAC AAC TCA CTT ACT CTC TTG AAG TAA GTG AGT TGT GGA ATG GGG |
| | |
| for site directed mutagenesis | |
| mCP2c (H312A)_F | GAA ACG GCT CGC CCA ACG CCC AGC CAG AAC CAC C |
| mCP2c (H312A)_R | GGT GGT TCT GGC TGG GCG TTG GGC GAG CCG TTT C |
| mCP2c (E315A)_F | CCA ACC ACC AGC CAG CAC CAC CCC CTC CAG TC |
| mCP2c (E315A)_R | GAC TGG AGG GGG TGG TGC TGG CTG GTG GTT GG |
| mCP2c (D322A)_F | CCC CTC CAG TCA CGG CTA ACC TCT TGC CGA C |
| mCP2c (D322A)_R | GTC GGC AAG AGG TTA GCC GTG ACT GGA GGG G |
| mCP2c (E332A)_F | CAA CCA CGC CTC AGG CAG CCC AGC AAT GGC TG |
| mCP2c (E332A)_R | CAG CCA TTG CTG GGC TGC CTG AGG CGT GGT TG |
| mCP2c (W336V)_F | CCT CAG GAA GCC CAG CAA GTG CTG CAT CGA AAC CGG |
| mCP2c (W336V)_R | CCG GTT TCG ATG CAG CAC TTG CTG GGC TTC CTG AGG |
| mCP2c (H338A)_F | GCC CAG CAA TGG CTG GCT CGA AAC CGG TTC TC |
| mCP2c (H338A)_R | GAG AAC CGG TTT CGA GCC AGC CAT TGC TGG GC |
| mCP2c (R339A)_F | CAG CAA TGG CTG CAT GCA AAC CGG TTC TCC AC |
| mCP2c (R339A)_R | GTG GAG AAC CGG TTT GCA TGC AGC CAT TGC TG |
| mCP2c (R341A)_F | CAA TGG CTG CAT CGA AAC GCG TTC TCC ACA TTC AC |
| mCP2c (R341A)_R | GTG AAT GTG GAG AAC GCG TTT CGA TGC AGC CAT TG |
| mCP2c (R347A)_F | GTT CTC CAC ATT CAC GGC GCT TTT CAC CAA CTT C |
| mCP2c (R347A)_R | GAA GTT GGT GAA AAG CGC CGT GAA TGT GGA GAA C |
| mCP2c (D356A)_F | CAA CTT CTC AGG GGC AGC TTT ACT GAA ACT AAC |
| mCP2c (D356A)_R | GTT AGT TTC AGT AAA GCT GCC CCT GAG AAG TTG |
| mCP2c (K359A)_F | GGG GCA GAT TTA CTG GCA CTA ACT AGA GAC GAC |
| mCP2c (K359A)_R | GTC GTC TCT AGT TAG TGC CAG TAA ATC TGC CCC |
| mCP2c (R362A)_F | GAT TTA CTG AAA CTA ACT GCA GAC GAC GTG ATC CAA ATC |
| mCP2c (R362A)_R | GAT TTG GAT CAC GTC GTC TGC AGT TAG TTT CAG TAA ATC |
| mCP2c (D363A)_F | CTG AAA CTA ACT AGA GCC GAC GTG ATC CAA ATC |
| mCP2c (D363A)_R | GAT TTG GAT CAC GTC GGC TCT AGT TAG TTT CAG |
| mCP2c (D364A)_F | GAA ACT AAC TAG AGA CGC CGT GAT CCA AAT CTG |
| mCP2c (D364A)_R | CAG ATT TGG ATC ACG GCG TCT CTA GTT AGT TTC |
| mCP2c (D373A)_F | CAA ATC TGC GGC CCT GCA GCT GGA ATC AGA CTC TTT AAT G |
| mCP2c (D373A)_R | CAT TAA AGA GTC TGA TTC CAG CTG CAG GGC CGC AGA TTT G |
| mCP2c (D376A)_F | CCT GCA GAT GGA ATC GCA CTC TTT AAT GCA TTA AAA G |
| mCP2c (D376A)_R | CTT TTA ATG CAT TAA AGA GTG CGA TTC CAT CTG CAG G |
| mCP2c (A380F)_F | GGA ATC AGA CTC TTT AAT TTC TTA AAA GGC CGG ATG G |
| mCP2c (A380F)_R | CCA TCC GGC CTT TTA AGA AAT TAA AGA GTC TGA TTC C |
| mCP2c (K382A)_F | GAC TCT TTA ATG CAT TAG CAG GCC GGA TGG TGC G |
| mCP2c (K382A)_R | CGC ACC ATC CGG CCT GCT AAT GCA TTA AAG AGT C |
| mCP2c (R384A)_F | CTT TAA TGC ATT AAA AGG CGC GAT GGT GCG GCC AAG |
| mCP2c (R384A)_R | CTT GGC CGC ACC ATC GCG CCT TTT AAT GCA TTA AAG |
| mCP2c (R387A)_F | CAT TAA AAG GCC GGA TGG TGG CGC CAA GGC TAA CCA TTT ATG |
| mCP2c (R387A)_R | CAT AAA TGG TTA GCC TTG GCG CCA CCA TCC GGC CTT TTA ATG |
| mCP2c (R389A)_F | CGG ATG GTG CGG CCA GCG CTA ACC ATT TAT GTC |
| mCP2c (R389A)_R | GAC ATA AAT GGT TAG CGC TGG CCG CAC CAT CCG |
| | |
| for reverse transcription quantitative PCR (RT-qPCR) | |
| mα-globin_qRT_F | GAT CCC AAG TTT TAC TCG GTA GAG CAA GCA CAA ACC AGG |
| mα-globin_qRT_R | GAT CCC TGG TTT GTG CTT GCT CTA CCG AGT AAA ACT TGG |
| hCP2c qRT_F | GGT TGG TGC AGG ACT TTG AT |
| hCP2c qRT_R | CAT GGA GTT TCA CTG CTG GA |
| hVIM qRT_F | GAA CCA ATG AGT CCC TGG AA |
| hVIM qRT_R | TCC AGC AGC TTC CTG TAG GT |

| | |
|---|---|
| hZEB1 qRT_F | GCA CAA CCA AGT GCA GAA GA |
| hZEB1 qRT_R | CAT TTG CAG ATT GAG GCT GA |
| hSNAI1 qRT_F | CCC CAA TCG GAA GCC TAA CT |
| hSNAI1 qRT_R | GAC AGA GTC CCA GAT GAG CA |
| hSNAI2 qRT_F | GTG TCC TTG AAG CAA CCA GG |
| hSNAI2 qRT_R | TGC GAT GCC CAG TCT AGA AA |
| hFN1 qRT_F | ACC AAC CTA CGG ATG ACT CG |
| hFN1 qRT_R | GCT GAT CAT CTG GCC ATT TT |
| hCD44 qRT_F | CAT CTA CCC CAG CAA CCC TA |
| hCD44 qRT_R | CCC AGA TGG AGA AAG CTC TG |
| hEGF qRT_F | CAG GGA AGA TGA CCA CCA CT |
| hEGF qRT_R | CAG TTC CCA CCA CTT CAG GT |
| hTGFA qRT_F | CTT TGG GGG TAT TGT GTT GG |
| hTGFA qRT_R | ACG TAC CCA GAA TGG CAG AC |
| hOCT4 qRT_F | GGT CCG AGT GTG GTT CTG TA |
| hOCT4 qRT_R | GGA AAG GGA CCG AGG AGT AC |
| hNANOG qRT_F | ACC CAG CTG TGT GTA CTC AA |
| hNANOG qRT_R | GGA AGA GTA AAG GCT GGG GT |
| hSOX2 qRT_F | AAC CCC AAG ATG CAC AAC TC |
| hSOX2 qRT_R | CGG GGC CGG TAT TTA TAA TC |
| hYY1 qRT_F | GAA TTT GCC AGA ATG AAG CC |
| hYY1 qRT_R | TCA TAG CAG AGT TAT CCC TG |
| hMDM2 qRT_F | CCT TCC ATC ACA TTG CAA CAG |
| hMDM2 qRT_R | CAG CTT GTG TTG AGT TTT CCA G |
| hp53 qRT_F | CGC TTC GAG ATG TTC CGA GA |
| hp53 qRT_R | CTT CAG GTG GCT GGA GTG AG |
| hp21 qRT_F | AGC CTG ACA GAT TIC TAT CAC |
| hp21 qRT_R | CTT TAA GTT TGG AGA CTG GGA |

for SNP detection

| | |
|---|---|
| hMDM2_SNP_F | TAG CAT TCC TGT GAC TGA GCA |
| hMDM2_SNP_R | GTC TAC ATA CTG GGC AGG GC |

for splicing detection

| | |
|---|---|
| hMDM2_Exon3_R | GGT TAC AGC ACC ATC AGT AGG |
| hMDM2_Exon12_F | GGA CAT CTT ATG GCC TGC TT |

for Chromatin immunoprecipitation quantitative PCR (ChIP-qPCR)

| | |
|---|---|
| hMDM2 enhancer 1_F | CAA CCT TCT CCT AAC CCT CAC |
| hMDM2 enhancer 1_R | CAA GGG TTG CAC TAC CGT G |
| hMDM2 enhancer 2_F | CTG TCT TCG GGT TAG GAG ATC |
| hMDM2 enhancer 2_R | CCC AAG TCC GCT AGC AG |
| hMDM2 promoter 3_F | CTT TTG GGT CTG GGC TCT G |
| hMDM2 promoter 3_R | AAC AAA ACC TCC GCA AAG C |
| hMDM2 promoter 4_F | GAG TTC AGG GTA AAG GTC ACG |
| hMDM2 promoter 4_R | CTG CAG TTT CGG AAC GTG |
| hFN 1-1 promoter_F | GGA CTG TGG GTT CGC AG |
| hFN 1-1 promoter_R | CCG CTT CCA TCC CTT C |
| hFN 1-2 promoter_F | TGG GAA GCC GAG TGT TTC |
| hFN 1-2 promoter_R | CCC AGA ATC AAT GAA TTT TAA GAA AGC |
| hFN 2 gene body_F | GGC CTA AAG AGG TCT GAA C |
| hFN 2 gene body_R | TGG TCC TTA CTG CTA CTT ATT TCC |
| hFN 3 CTCF_F | GAG CTG TTT GGT CTC GAC TC |
| hFN 3 CTCF_R | AAA GGT TAA TTC AGT ACA AGG TGC |
| hFN 4 intergenic_F | GCC TTG AAG AGA GTA GTG GTT C |
| hFN 4 intergenic_R | GTG TGA GGT GTC AGT CTC GC |
| hVIM 1 promoter_F | AAG ATG TAA CTC AGA GCA TAG GC |
| hVIM 1 promoter_R | CTC TTT CAC TGG GAG GCT G |
| hVIM 2 gene body_F | CCG CGT TCC AAT CTC AGG |
| hVIM 2 gene body_R | GGA AAG AGT AAG GAA TCC CTC AG |
| hVIM 3 CTCF_F | GGG TTC GGA AGT CAC AGG |
| hVIM 3 CTCF_R | GAA TGC CTA ATT GTA TCC ACT GG |
| hVIM 4 intergenic_F | GAG GAC ATG AGA TTT GGG AGG |
| hVIM 4 intergenic_R | CCA GGT TTT GCT CTT GAC ATA TG |

siRNA

| | |
|---|---|
| hTHBS siRNA | Santa Cruz, sc-36665 |
| hADM siRNA | Santa Cruz, sc-39273 |
| hTP53I3 siRNA | Santa Cruz, sc-36223 |
| hID3 siRNA | Santa Cruz, sc-38002 |
| hKLF10 siRNA | Santa Cruz, sc-45463 |
| hTNFRSF12A siRNA | Santa Cruz, sc-43764 |
| hGCLM siRNA | Santa Cruz, sc-40603 |

**Table S3.**

Drug & peptide list

| name | Cat # or sequence |
|---|---|
| Sorafenib | Sigma-Aldrich, SML2653 |
| CASP2 inhibitor | Ac-VDVAD-CHO |
| iRGD | CRGDKGPDC |
| CP2 1P | QEAQQWLHRNRFS |
| CP2 2P | FSGADLLKLTRDD |
| CP2 3P | ICGPADGIRLFNA |
| CP2 4P | VRPRLTIYVCQES |
| PEP #5 | HERRESNYPQRP |
| Pep #8 | HNMHKHSASRIH |
| Pep #21 | HKFHQHRLPHLA |
| Pep #5-1 | HERRES |
| Pep #5-2 | NYPQRP |
| Pep #5-A | Ac-HERRESNYPQRP-NH2 |
| Pep #5-B | HERRESNYPQRPCRGDKGPDC |
| Pep #5-C | Ac-HERRESNYPQRPCRGDKGPDC-NH2 |
| Pep #5-2A | Ac-NYPQRP-NH2 |
| Pep #5C (ACP5C) | Ac-HERRESNYPQRPCRGDKGPDC-NH2 |
| Pep #5-2C (ACP52C) | Ac-NYPQRPCRGDKGPDCK-NH2 |
| Biotin-Pep #5-2A | Ac-NYPQRPGGK(biotin)-NH2 |
| Biotin-Pep #5-2C (ACP52CB) | Ac-NYPQRPCRGDKGPDCK(biotin)-NH2 |
| Cy5-ACP52C | cy5.5-aca-NYPQRPCRGDKGPDC-NH2 |
| ACP52-51C | Ac-NYPQRCRGDKGPDC-NH2 |
| ACP52-52C | Ac-YPQRPCRGDKGPDC-NH2 |
| ACP52-4C | Ac-YPQRCRGDKGPDC-NH2 |
| ACP52-4C/1F | Ac-FPQRCRGDKGPDC-NH2 |
| ACP52-4C/1S | Ac-SPQRCRGDKGPDC-NH2 |
| ACP52-4C/1T | Ac-TPQRCRGDKGPDC-NH2 |
| ACP52-4C/2G | Ac-YGQRCRGDKGPDC-NH2 |
| ACP52-4C/3N | Ac-YPNRCRGDKGPDC-NH2 |
| ACP52-4C/4K | Ac-YPQKCRGDKGPDC-NH2 |
| ACP52-31C | Ac-YPQCRGDKGPDC-NH2 |
| ACP52-32C | Ac-PQPCRGDKGPDC-NH2 |
| ACP52D | Ac-KIKKVKKKGRKGSKIKKVKKKGRKGGNYPQRP-NH2 |
| ACP52CG | Ac-K(E-pal)K-GGNYPQRPCRGDKGPDC-NH2 |
| ACP52CK | Ac-K(EGFLG-pal)K-GGNYPQRPCRGDKGPDC-NH2 |
| DHA-ACP52C | DHA-GGNYPQRPCRGDKGPDC-NH2 |
| ACP52GK | Ac-NYPQRPGG-K(E-pal)-GGCRGDKGPDC-NH2 |
| ACP52CGK | Ac-NYPQRPGG-K(γE-pal)-GGCRGDKGPDC-NH2 |
| ACP52CGK-α1 | Ac-NYPQRPGGVDVADGGNYPQRPGG-K(γE-pal)-GGCRGDKGPDC-NH2 |

| | |
|---|---|
| ACP52CGK-α2 | Ac-NYPQRPGGGFLGVDVADGGNYPQRPGG-K(γE-pal)-GGCRGDKGPDC-NH2 |
| ACP52CGK-α3 | Ac-NYPQRPGGVDVADGFLGGGNYPQRPGG-K(γE-pal)-GGCRGDKGPDC-NH2 |
| ACP52CGK-α4 | Ac-NYPQRPGGNYPQRPGG-K(γE-pal)-GGCRGDKGPDC-NH2 |
| Cy5-ACP52CGK | cy5.5-aca-NYPQRPGG-K(γE-pal)-GGCRGDKGPDC-NH2 |

**Table S4.**
Antibody list

| immunogen (species) | company | cat # |
|---|---|---|
| CP2c (human) | Abcam | ab155238 |
| CP2c (human) | BD Biosciences | 610818 |
| CP2b (human) | Santa Cruz | sc-81310 |
| pCDK1 (human) | Cell Signaling | 9114 |
| CDK1 (human) | Upstate | 06-923 |
| CDK2 (human) | Santa Cruz | sc-163 |
| CDK4 (human) | Upstate | 06-139 |
| cyclin A (human) | Abcam | ab38-100 |
| cyclin B1 (human) | Abcam | ab72-100 |
| cyclin D (human) | Santa Cruz | sc-8396 |
| cyclin E (human) | Santa Cruz | sc-198 |
| CHK1 (human) | Santa Cruz | sc-7898 |
| CDC25c (human) | Santa Cruz | sc-13138 |
| p21 (mouse) | Santa Cruz | sc-6246 |
| p53 (human) | Santa Cruz | sc-126 |
| ACTB (human) | Santa Cruz | sc-1616 |
| MCL1 (human) | Santa Cruz | sc-819 |
| BCL2 (human) | BD Biosciences | 551109 |
| BCL-XL (human) | Abcam | ab38629 |
| BIM (human) | Santa Cruz | sc-11425 |
| BAX (human) | BD Biosciences | 556467 |
| BAK (human) | EMD | AM03 |
| ProCASP3 (human) | Cell Signaling | 9665 |
| Cleaved CASP3 (human) | Cell Signaling | 9661 |
| ProCASP8 (human) | Santa Cruz | sc-7890 |
| ProCASP9 (human) | Santa Cruz | sc-7885 |
| ProCASP11 (mouse) | Santa Cruz | sc-15881 |
| ProCASP12 (mouse) | Santa Cruz | sc-5627 |
| p73 | Abcam | ab189896 |
| p63 (human) | Abcam | ab110038 |
| YY1 (human) | Santa Cruz | sc-7341 |
| MDM2 (human) | Santa Cruz | sc-5304 |
| MDM2 (human) | Genetex | GTX100531 |
| MDM2 (human) | Abcam | ab226939 |
| PSME3 (human) | ZYMED | 383800 |
| SUMO1 (human) | Santa Cruz | sc-5308 |
| PIAS1 (human) | Abcam | ab32219 |
| H2AX | Abcam | ab11175 |
| pATM (human) | Abcam | ab81292 |
| CHK2 (human) | Ab Frontier | LF-PA20083 |
| pCHK2 (human) | Ab Frontier | LF-PA20084 |
| ATM (human) | Santa Cruz | sc-135663 |
| TDP2 (human) | Santa Cruz | sc-377280 |
| ATR (human) | Ab Frontier | LF-PA20681 |
| pATR (human) | Abcam | ab227851 |
| pCHK1 (human) | Ab Frontier | LF-PA20082 |
| FBXO31 (human) | Abcam | ab68067 |
| HA | Abcam | ab49969 |
| Flag | Abcam | ab2493 |
| EGFP | Abcam | ab5449 |
| BrdU | Santa Cruz | sc-32323 |
| Hsp60 | Ab Frontier | YF-PA12436 |
| LC3 | Ab Frontier | LF-PA22271 |
| FLAG-M2 | Abcam | ab49763 |
| anti-rabbit IgG-HRP | Ab Frontier | LF-SA8002 |
| anti-mouse IgG-HRP | Thermo Fisher | 31430 |
| anti-goat IgG-HRP | Invitrogen | 811260 |
| anti-mouse IgG-Cy3 | Vectorlabs | CY-2300 |

| | | |
|---|---|---|
| anti-rabbit IgG-FITC | Vectorlabs | FI-1000 |
| anti-goat IgG-FITC | Vectorlabs | CY-2500-1 |